HHS Public Access

Author manuscript

Neuroimage. Author manuscript; available in PMC 2023 April 01.

Published in final edited form as:

Neuroimage. 2022 April 01; 249: 118863. doi:10.1016/j.neuroimage.2021.118863.

Using diffusion tensor imaging to effectively target TMS to deep brain structures

Bruce Luber, PhD[a,b,*], **Simon W. Davis, PhD**[c,*], **Zhi-De Deng, PhD**[a,b], **David Murphy, MS**[b], **Andrew Martella, MD**[b], **Angel V. Peterchev, PhD**[b,d,e,f], **Sarah H. Lisanby, MD**[a,b]

[a]Noninvasive Neuromodulation Unit, Experimental Therapeutics & Pathophysiology Branch, National Institute of Mental Health, National Institutes of Health, Bethesda, MD

[b]Department of Psychiatry & Behavioral Sciences, Duke University School of Medicine, Durham, NC

[c]Department of Neurology, Duke University School of Medicine, Durham, NC

[d]Department of Biomedical Engineering, Duke University, Durham, NC

[e]Department of Electrical and Computer Engineering, Duke University, Durham, NC

[f]Department of Neurosurgery, Duke University School of Medicine, Durham, NC

Abstract

TMS has become a powerful tool to explore cortical function, and in parallel has proven promising in the development of therapies for various psychiatric and neurological disorders. Unfortunately, much of the inference of the direct effects of TMS has been assumed to be limited to the area a few centimeters beneath the scalp, though clearly more distant regions are likely to be influenced by structurally connected stimulation sites. In this study, we sought to develop a novel paradigm to individualize TMS coil placement to non-invasively achieve activation of specific deep brain targets of relevance to the treatment of psychiatric disorders. In ten subjects, structural diffusion imaging tractography data were used to identify an accessible cortical target in the right frontal

Corresponding Author: Bruce Luber, Ph.D., bruce.luber@nih.gov.
*These authors contributed equally to this work.

Credit Author Statement
Bruce Luber: Methodology, Formal Analysis, Writing: Original Draft
Zhi-De Deng: Writing: Review & Editing, Formal Analysis
David Murphy: Investigation, Software, Methodology, Writing: Review & Editing, Formal Analysis
Simon Davis: Methodology, Writing: Review & Editing, Formal Analysis
Andrew Martella: Investigation, Methodology, Writing: Review & Editing, Formal Analysis
Angel Peterchev: Supervision, Project Administration, Writing: Review & Editing, Conceptualization, Methodology
Sarah H. Lisanby: Resources, Supervision, Project Administration, Funding Acquisition, Writing: Review & Editing, Conceptualization, Methodology

*Data and Code Availability Statement
Data and code availability
The data that support the findings of this study are from the corresponding author, Bruce Luber, upon reasonable request. Researchers wishing to obtain the data must contact the Office of Research Contracts at Duke University School of Medicine to initiate a discussion on the proposed data transfer or use.

pole that demonstrated both anatomic and functional connectivity to right Brodmann area 25 (BA25). Concurrent TMS-fMRI interleaving was used with a series of single, interleaved TMS pulses applied to the right frontal pole at four intensity levels ranging from 80% to 140% of motor threshold. In nine of ten subjects, TMS to the individualized frontal pole sites resulted in significant linear increase in BOLD activation of BA25 with increasing TMS intensity. The reliable activation of BA25 in a dosage-dependent manner suggests the possibility that the careful combination of imaging with TMS can make use of network properties to help overcome depth limitations and allow noninvasive brain stimulation to influence deep brain structures.

Keywords

TMS; connectivity; diffusion imaging tractography; targeting; deep brain stimulation; subgenual cingulate cortex

1.1. Introduction

In the past few decades, transcranial magnetic stimulation (TMS) has developed into a powerful tool for causally establishing brain-behavior relationships, specifically in exploring cortical function. In parallel, its neuromodulatory effects have proven promising for the development of therapies for various psychiatric and neurological disorders, notably gaining FDA approval in 2009 for the treatment of major depressive disorder (MDD), and more recently, obsessive-compulsive disorder (OCD). The basis for this wide application is that TMS reliably modulates cerebral activity. However, the extent and distribution of this cortical or subcortical response has yet to be fully appreciated, and one of the most promising trends in both the clinical and basic science applications of TMS is the appreciation of neural effects extending well beyond the site of stimulation.

Used in conjunction with brain imaging, newer methods of TMS targeting have been developed which greatly increase the effect of TMS on neural processing (Sack et al., 2009). Coil positioning can be guided using infrared devices, coil location can be co-registered with an individual's structural MRI and fMRI, and robotic coil holders can hold position relative to the target, adaptively compensating for subject movements during the stimulation period. All of these technical developments have led to TMS targeting with millimeter resolution focused on functionally active areas specific to each individual. Unfortunately, this precision targeting is subject to a serious conceptual limitation: TMS can only directly stimulate superficial cortex effectively, with an approximately 3 cm maximum depth from the surface of the head at which the most commonly used coil- the figure-8 coil- can cause neuronal firing (Deng et al., 2013; Figure 1). Yet the ability to quantify our ability to affect deeper targets to stimulate anywhere in the brain noninvasively obviously would make TMS a much more powerful research tool for probing neural circuitry. To be sure, it is likely that extant applications of TMS act through their structural and functional connectivities to other regions; but absent any consistent method for identifying the routes to subcortical targeting, the field is limited. Moreover, a systemic framework for noninvasive focal deep brain stimulation would likely prove valuable in therapeutic neuromodulation. Certainly invasive focal deep brain stimulation (DBS) of subcortical structures has been transformative in

the treatment of neurological illnesses such as Parkinson's Disease, dystonia, and essential tremor (Kringelbach et al., 2007), and in psychiatric disorders, has shown great promise for treatment of OCD (Mian et al., 2010) and is currently being investigated in MDD (Dougherty, 2018).

The primary TMS depression target- dorsolateral prefrontal cortex (DLPFC)- is located in superficial cortex, a relatively accessible patch of cortex that can be stimulated with electric-fields (E-fields) averaging 92 V/m under typical treatment conditions (Deng et al., 2019). The efficacy of TMS to DLPFC in 4 pivotal trials that led to FDA approval for depression was only moderate: 14% remission with active TMS compared to 9% with sham TMS at 6 weeks (O'Reardon et al., 2007), and 14% remission with active TMS and 5% with sham TMS (George et al. 2010), respectively, although using structural imaging guidance for TMS coil placement and other methodologies has slightly improved outcomes (Fitzgerald et al., 2009; Carpenter et al., 2012). Anatomical studies of the neurocircuitry of mood disorders have indicated that other therapeutic targets may be deeper within the brain (Mayberg et al., 2005). Tract-tracing studies in animals and diffusion tensor imaging (DTI) studies in humans suggest that DLPFC has limited direct connectivity with critical nodes in the depression neurocircuit (Price and Drevets, 2010; Gutman et al., 2009; Haber et al., 2006; Haber and McFarland, 1999), such as subcallosal cingulate (SCC or BA25) white matter (Johansen-Berg et al., 2008; Gutman et al., 2009) and ventral capsule/ventral striatum (Malone et al., 2009; Greenberg et al., 2006). While anatomical connectivity may not be strong between DLPFC and BA25, there is evidence that a functional association may exist between them that is related to depression (Fox et al., 2012) and to treatment using TMS (Hadas et al., 2019). Thus, a more direct targeting of BA25 (the primary target of most surgical DBS applications) relying on the structural connections to this region may prove potentially beneficial. However, lacking a method to guide TMS coil placement to access deep brain targets limits the utility of TMS in studying and treating disorders with heavy involvement of medial and deep structures.

Fortunately, there is an increasing awareness that TMS can evoke action potentials not only cortex directly beneath the TMS coil, but in remote regions within the cortical network connected to the stimulation site. Evidence supports transsynaptic action of superficial TMS into deep brain regions. TMS studies utilizing concurrent neuroimaging with fMRI (Baudewig et al., 2001; Bestmann et al., 2003; Roberts et al., 1997; Bohning et al., 1998; Davis et al., 2017; Tik et al., 2017), PET (Fox et al., 1997; Ferrarelli et al., 2004), and EEG (Ilmoniemi et al., 1997), have demonstrated that TMS stimulation of superficial cortical targets can result in measurable effects at remote sites including those that are deep relative to the surface of the brain such as the hippocampus and other limbic regions (Denslow et al., 2005; Li et al., 2004; Bestmann et al., 2004; Wang et al., 2018). For example, TMS of the motor cortex induced measurable dopamine release in the putamen while rTMS of the DLPFC induced dopamine release in the head of the caudate (Strafella et al., 2003, 2005; Cho & Strafella, 2009). Studies using concurrent TMS– fMRI reported effects in BA25/12, orbitofrontal cortex, caudate, amygdala, and thalamus, when stimulating the DLPFC (Fonzo et al., 2017; Oathes et al., 2018; Vink et al., 2018; Dowdle et al., 2018). Such results have led to the suggestion that TMS can be used to take explicit advantage of transsynaptic effects in a targeted fashion, and that MRI measures of connectivity could be used to guide

cross-network targeting (Fox et al., 2012, 2013; Weigand et al., 2018), and a number of studies have used task-based functional connectivity MRI (Bien et al., 2009; de Graaf et al., 2009; Zanto et al., 2011), and DTI (Hannula et al., 2010), to find cortico–cortical pathways to target more distant cortical regions with TMS.

In this study, we sought to develop a paradigm to individualize TMS coil placement based on structural connectivity to non-invasively achieve activation of deep brain targets of relevance to the treatment of psychiatric disorders. Specifically, diffusion imaging tractography was used in order to identify a noninvasively accessible cortical TMS target in the frontal pole that demonstrated anatomic connectivity to BA25. Following this, interleaved TMS-fMRI was used to verify both functional connectivity between the superficial and deep target and successful activation of BA25, specifically examining dose-response relations between TMS intensity and BOLD response in the remote target.

1.2. Methods

1.3. Subjects

Twelve healthy subjects (6 female, 6 male, age 19 years to 33 years, 4 left-handed) were recruited and provided written informed consent for the study, which was approved by the Duke University School of Medicine Institutional Review Board. All subjects were screened for psychiatric disorders, substance abuse/dependence, a history of neurological disease, pregnancy, or seizure risk factors. Results from two subjects were excluded from analysis because one had an anatomical anomaly discovered during MRI acquisition and the other because the coil moved during acquisition of interleaved TMS-fMRI scans.

1.4. Procedure

Two separate MRI sessions were conducted after initial screening and consenting. In the first session, anatomical, functional, and DTI data sets were acquired. A target for cortical TMS was determined from analysis of the diffusion and anatomical imaging data. In the second session, interleaved TMS–fMRI was performed using this target, measuring BOLD signal changes during application of single-pulse TMS at the diffusion tractography determined stimulation site.

1.5. First Session MRI Acquisition

All imaging data were acquired on a GE MR 750 3 Tesla scanner. First session data was acquired with a 8 HR Brain coil. High resolution structural, diffusion-weighted imaging, and resting-state fMRI were acquired. Structural MRI data was obtained using a gradient echo sequence with parameters including a flip angle = 77, repetition time (TR) = 1750 ms, echo time (TE) = 27 ms, field of view (FOV) = 22 mm^2, and 39 4-mm thickness slices. Diffusion-weighted imaging data was obtained using a single-shot, spin echo planar sequence with parameters including a TR = 9000 ms, TE = minimum, FOV = 25.6 mm^2, and 68 2-mm thickness slices, and with b-value = 1000. Thirty directions of diffusion gradients were used. For resting-state fMRI, we collected 2 runs of 158 contiguous EPI functional volumes (TR = 1750 ms; TE = 30 ms; flip angle = 90, 38 slices, matrix = 64 × 64; FOV = 192 mm; acquisition voxel size = 3 × 3 × 3 mm^3). During the scans, subjects were

instructed to rest with eyes open while the word “Relax” was projected center-screen in white against a black background. imaging, and resting-state fMRI were acquired. Structural MRI data was obtained using a gradient echo sequence with parameters including a flip angle = 77, repetition time (TR) = 1750 ms, echo time (TE) = 27 ms, field of view (FOV) = 22 mm^2, and 39 4-mm thickness slices. Diffusion-weighted imaging data was obtained using a single-shot, spin echo planar sequence with parameters including a TR = 9000 ms, TE = minimum, FOV = 25.6 mm^2, and 68 2- mm thickness slices. Thirty directions of diffusion gradients were used. For resting-state fMRI, we collected 2 runs of 158 contiguous EPI functional volumes (TR = 1750 ms; TE = 30 ms; flip angle = 90, 38 slices, matrix = 64 × 64; FOV = 192 mm; acquisition voxel size = 3 × 3 × 3 mm^3). During the scans, subjects were instructed to rest with eyes open while the word “Relax” was projected center-screen in white against a black background.

1.6. Target Localization

The target location for seed-based tractography in subcallosal-cingulate white matter near BA25 was determined for each subject using the T1 weighted anatomical image, applying an algorithm used for the surgical placement of electrodes in patients receiving DBS (Hamani et al., 2009; see Figure S1). Using anatomical boundaries that constrained tractography (posterior: anterior commissure; anterior: Brodmann Area 10) one line was drawn on the most ventral surface of the frontal lobe and another line to designate the anterior commissure. These first two lines provided anatomical boundaries. Thereafter, an anterior-posterior line extending from the anterior commissure to the anterior surface of the corpus callosum was drawn. A dorsal-ventral line extending from the inferior surface of the corpus callosum to the ventral surface of the frontal lobe was drawn. The anterior-posterior line and dorsal-ventral line were both divided into quartiles, and a region corresponding with 70–75% of the anterior-posterior line and 25–30% of the dorsal ventral line was identified. This intersecting point served as the defined target of interest. A seed mask defining the ROI was drawn with its center at this location. The mask was 2 cm in diameter and 5 sagittal slices thick. Once drawn, the seed region coordinates were transferred into the diffusion data space by applying a transformation matrix produced by registration of the anatomical image to the unstripped, unweighted (b0) image from the diffusion data. Seed masks were drawn by hand by two expert raters, who performed ROI quantification on a subset of samples to ensure consistency in seed definition, and attained an high interclass coefficient of 0.85.

1.7. Diffusion Imaging Analysis

Diffusion imaging data were analyzed separately for each individual using tools from FSL 4.1 (www.fmrib.ox.ac.uk/fsl/). Diffusion-weighted images were visually inspected for systemic artifacts due to excessive motion, EPI distortions, or signal dropout, and when possible were corrected using eddy correction of implicit application of the phase encoding map. Bayesian Estimation of Diffusion Parameters (BEDPOST) were then performed on the full set of diffusion data, which performs an affine registration in order to correct for current-induced shearing or subject movement-related distortions, and the resulting images were then skull-stripped to remove all non-brain voxels. Next, vector orientations were rotated to match the coregistration parameters inherent in the previous step. Then, a standard tensor model was fit at each voxel using the Functional MRI of the Brain’s Diffusion

Toolbox (FDT; www.fmrib.ox.ac.uk/fsl), in order to create fractional anisotropy (FA) maps for each subject. Next, FSL's probtrackx tool was used to perform probabilistic tractography with the now coregistered tracing as a seed. Standard parameters for tractography were used; each voxel within the seed mask was seeded with 5000 streamline samples that migrated according to a step length of 0.5mm, a curvature threshold of 0.2, and a "loopcheck" to exclude tracks that double back on themselves. FA maps in the diffusion space were then coregistered with the anatomical space for the location of stimulation site, in order to provide transformation between diffusion and structural space (both within native space). As described below, tractography indicated that the right frontal pole was the nearest TMS-accessible cortex connected to the seed region via diffusion tractography. Thus the frontal pole site nearest to the anterior terminus of the tractography path was selected as the desired stimulation target in each subject.

1.8. Seed-based functional connectivity analysis

Based on the time series of a seed voxel (or ROI), connectivity was calculated as the correlation of time series for all other voxels in the brain. Image preprocessing consisted of: (1) slice time correction for interleaved acquisitions, (2) motion correction (using a twelve parameter nonlinear affine transformation implemented in FNIRT), (3) spatial smoothing (Gaussian kernel of FWHM = 6 mm), (4) temporal high-pass filtering (Gaussian-weighted least-squares straight line fitting with sigma = 100.0 s), and (5) low-pass temporal filtering (Gaussian filter with HWHM = 2.8 s). The functional scans were corrected for small (< 2mm) head movements by realigning all functional scans to the first functional volume. BA25 ROIs used in the tractography analysis above were transformed to standard MNI space, and we calculated the mean time-series for the BA25 ROI within the two first session rest scans. Individual analyses of functional connectivity were carried out for each participant using multiple regression (as implemented in FSL's FEAT). The regression model included the BA25 time-series as predictors as well as the nuisance covariates (seed time- series for global signal, white matter, cerebrospinal fluid, and six motion parameters). In order to identify the functional connectivity-based cortical target, we identified the location on the cortical surface that was (1) was in in frontal cortex, (2) was closest to the scalp, and (3) had a z-score > 2.3. Locations were marked for MNI coordinate for later comparison with tractography-based targets. Group-level analyses were carried out using a mixed-effects model (FLAME) as implemented in FSL. Corrections for multiple comparisons were carried out at the cluster level using Gaussian random field theory (min $z > 2.3$; cluster significance: $p < 0.05$, corrected). This group-level analysis produced thresholded z-score maps of activity associated with functional connectivity to the target region.

2.2.5. Interleaved TMS-fMRI Session—For the interleaved TMS-fMRI session, the TMS targets in the frontal pole were derived separately for each subject based on their individual tractography data. Tractography-based targets demonstrated a greater spatial precision in frontopolar cortex compared to compared to functionally-based targets (see mean eccentricity estimates below), and therefore the generalizability of TMS to this frontal location. Post-hoc analyses described below relate this eccentricity to the size of the TMS effect in BA 25. Prior to the TMS-fMRI session, the scalp location for TMS

coil position over the frontal pole had been found by coregistering the tractography paths to the subject's head using an infrared frameless stereotaxy system (BrainSight: Rogue Research, Montreal, Canada). The location was marked on a tight fitting acrylic swim cap that stayed on the subject's head until TMS-fMRI interleaving was completed on the same day. At that time, subjects were acclimated to TMS with a series of single pulses at the target site. In the scanner room, the motor threshold (MT) for each subject was determined using a MagVenture R30M device located outside the scanner room, part of an MRI compatible TMS system which included a non-ferrous figure-8 coil with 12 m long cable and artifact reducing counter-current charging system (MagVenture, Farum, Denmark). MTs were determined using electromyography of the right first dorsal interosseous (FDI) muscle and defined as the lowest setting of TMS device intensity at which at least 5 out of 10 motor evoked potentials were ≥ 50μV peak to peak. The TMS coil was then positioned over the individual's marked right medial frontal pole target site and locked into place using a coil holder provided as part of the MagVenture system, and subjects were then positioned in the scanner. Four runs of interleaved TMS-fMRI were then performed. In each run, single TMS pulses were delivered between 8 and 12 seconds apart. The interstimulus periods were pseudo-randomly sequenced such that the mean ISI was 10 s, and the total run time was 400 s. The intensity of the biphasic pulse varied between 4 levels: 80%MT, 100%MT, 120%MT, and 140%MT. The intensity for each pulse was pseudo-randomly determined, with the limitation that the total number for each intensity be 10 pulses per run. In each interleaved TMS/fMRI scanning session, there were therefore 40 pulses per intensity level, for a total of 160 pulses across all runs.

Imaging data were acquired using a gradient echo sequence with the following imaging parameters: *flip angle = 77°, TR = 1750ms, TE = 27ms, FOV = 25.6 mm*^{2}, and *field of view (FOV) = 22 mm*^{2}, and *39 4-mm* thickness slices. These data were collected with a GE three-axis balanced- torque head gradient coil and a shielded end-capped quadrature transmit-receive birdcage radio frequency coil; consequently, the imaging sequence was distinct from the resting state data above. A delay of 250 ms was inserted between each acquisition, giving an "apparent" TR of 2000ms during which a single biphasic TMS pulse was delivered during the middle of this delay, ~125ms after the onset of the delay. The synchronization of TMS pulses with EPI acquisitions was achieved with a National Instruments NIUSB-6009 data acquisition module. MATLAB (Mathworks, Cambridge, MA) was used to read the scanner trigger pulses, to control both amplitude and stimulation triggers of the TMS device via serial communication, and record the timing of each event. To track the actual position of the coil during interleaved TMS-fMRI, four identical fiducial markers (8mm round non-metallic Liquimark markers, MRIEquip) were placed on the surface of the coil such that their centroid was at the center of the coil. In the MRIs, the mean coil location in standard space was calculated by first locating the four fiducial markers in the native-space anatomical scans acquired immediately before and after the interleaved TMS-fMRI session. Then, by calculating the center-point of all 4 markers, we calculated the centroid reflecting the focal point of the TMS coil; we then calculated the difference between the planned stimulation location (as determined by diffusion tractography) and the effective stimulation location (which may vary slightly during the course of the TMS/fMRI scan.

2.3. Data Analysis

2.3.1. Group DTI Analysis—In order to summarize the group anatomical tracts explored in the current study, individual tractography maps from the target site were transformed into the standard space of the MNI152 T1–2mm template image by using FLIRT and applying the normalization parameters from a tract- based normalization algorithm (tract-based spatial statistics; fsl.fmrib.ox.ac.uk/fsl/fslwiki/TBSS). The group results were then prepared by first averaging non-zero FA scores for all subjects and then selecting voxels with FA scores three standard deviations above the result of that average. Voxels that survived this threshold were then binarized to create a region of interest mask for later group- level functional analysis.

2.3.2. fMRI Analysis—Functional imaging analysis was carried out with FEAT (FMRI Expert Analysis Tool) Version 5.1from FSL (FMRIB's Software Library). Additional statistical analysis was performed in MATLAB (Mathworks, Cambridge, MA). All subject-level data was corrected for head motion (6 motion parameters, plus temporal derivatives and their squares), slice time corrected, smoothed with an 8mm kernel, high-pass and low-pass filtered as above, and pre-whitened. BOLD signal changes as a result of stimulation at 80%MT, 100%MT, 120%MT, and 140%MT were modeled with a general linear model (GLM) with each amplitude serving as an independent variable. Temporal derivatives were included in the model to allow for slight variations in the onset of the HRF for each condition. Higher level analysis was carried out in FEAT, using a fixed effects model and individual z-statistic maps were created using a cluster correction thresholded to $z > 1.65$ and with a cluster extent threshold of $p < 0.05$.

Our primary analysis focused on an a priori regions of interest comprising both the site of stimulation, putative deep-brain target regions, and a control region. Four regions were defined: one around BA25 based on the group tractography results from the seed in the right hemisphere, the corresponding region in the contralateral (left) hemisphere, a spherical region ($r = 25mm$) placed at the group averaged stimulation site of each subject, and another spherical ($r = 25mm$) region placed at a central dorsal site that showed little to no connection to the seed BA25 target to serve as a control region (Figure 2). Any voxels in the tractography based ROI that overlapped with the stimulation site spherical ROI were removed. All z-score maps used for this analysis were cluster corrected to a $z > 2.3$ and a cluster significance of $p < 0.05$ in FSL. Group analysis of the ROIs was carried out using FLAME (FMRIB's Local Analysis of Mixed Effects), estimating the group average activation patterns from the subject level z-statistic maps. z-statistic maps were cluster corrected to a threshold of $z > 1.65$ with a cluster extent threshold of $p < 0.05$ for the *Rest* contrasts and a threshold of z > 2.0 with a cluster extent threshold of $p < 0.05$ for the 80%MT contrasts. The dependence of the number of significant voxels within each ROI on stimulation amplitude was also modeled. The anatomical regions associated with the activation clusters were determined in MRIcron (http://www.mccauslandcenter.sc.edu/mricro/mricron/).

To evaluate distal regions of activation, whole brain analysis was carried out using the same steps as in the Group analysis but z-statistic maps were thresholded to z > 1.65 with a cluster

extent threshold of $p < 0.05$. Again anatomical regions associated with the whole brain maps were determined with MRIcron.

2.4. Guided Principal Component Analysis

While the group analyses depicted above provide estimates of the generalizability of the stimulation effect, we sought to determine the specificity of the result within individual subjects using a within-subjects method that identifies patterns of regional functional connectivity that exhibit increased activity across graduated changes in stimulus intensity. The event-related fMRI data were analyzed using the ordinal trends covariance model (OrT) in order to extract a pattern of activity that increased monotonically with TMS pulses of increasing intensity. OrT is described and validated in Habeck et al. (2005) and Moeller and Habeck (2006) and has been used successfully in previous fMRI analyses in TMS studies (e.g., Luber et al., 2008). OrT aims to identify topographic patterns that express ordinal trends on a subject-by-subject basis. OrT is a guided principal components analysis: a specially designed linear transformation is applied to the neuroimaging data with the effect that maximal salience is assigned to topographic patterns whose expressions are monotonic across a specified series of experimental conditions, corresponding to the positive incremental changes expected in the level of the targeted neural signal. The specific details of the analysis can be found in Habeck et al. (2005).

The OrT analysis was performed in MATLAB using a program package provided by Christian Habeck, James Moeller and Tony Ng of Columbia University. Voxel-wise data for each subject across three conditions were input to the guided PCA. The three conditions were the 80% condition, which provided a sub-threshold baseline, and data at 120% and 140% MT, chosen as the two conditions which showed significant activation of BA25 in contrasts with that baseline. The output of the PCA is a set of components, each composed of an eigenimage and associated subject scores for that image for each of the three conditions. A linear regression model fitting procedure was performed to find a combination of components that produced the least number of exceptions to a monotonic increase in combined weighted subject scores from the baseline condition to the 140%MT condition. A restriction was placed on the sets of components chosen to be tested: they could only be contiguous (first component, first and second component, first second and third components) in order to ensure a best fitting combined component that accounts for a good amount of variance. Akaike's Information Criterion (AIC) was used to estimate the best model fit, i.e. the best trade-off between over- and under-fitting the outcome measure (i.e., the number of exceptions): with the best model being the one producing the lowest AIC. A permutation test was then performed on the best fitting model to approximate a p-value for it. The original images were permuted across condition for each subject to gather information on the number of exceptions to a monotonic increase in subject scores. An OrT analysis was performed on each permuted sample, as on the original image set. Two hundred analyses of these permuted images were performed. Leading to a distribution in exception values, and the p-value being the relative frequency of the permuted exception values exceeding that of the best fit model. To test the robustness of voxel loadings in the pattern associated with the best-fit model, a bootstrapping procedure was used. The data were resampled without breaking the subject-condition assignment, and the test estimated the natural variability

under the real distribution that the sample was drawn from. The algorithm that produced the loadings in the pattern associated with the best-fit model was applied to resampled data over 500 iterations, leading to a normally distributed z-statistic for every voxel. This z-statistic gave an estimate of reliability of the voxel weight in the best-fit pattern.

2.5. Comparison of Structural and Functional Targets

Lastly, we sought to compare the within-subject reliability of either structurally or functionally-defined targets (based upon seed-based correlations using either tractography or functional connectivity) to predict the activity see in our target site, subgenual cortex. This within-subject reliability reflects the degree to which we “hit our target”, i.e., the effective stimulation site in the scanner matched the planned stimulation target as computed with either structural or functional connectivity analyses. We first summarized the stimulation effect across all subjects by calculating the linear slope of a line predicting component size reflecting the effect in BA25 at each of three stimulation intensities (80%, 120%, 140% MT). Euclidean distance from the center of gravity of the stimulation spheres to either the tractography-based targets or functional connectivity targets was calculated, and compared to the stimulation effect in order to determine if the proximity of the stimulation spheres to either the tractography- or functional connectivity-based targets best predicted the size of the stimulation effect. Thus, a significant negative slope suggests that if we had closed the distance between the planned and actual stimulation site (during the in-scanner positioning, which can be cumbersome), a stronger effect in BA25 might have been observed.

1.9. Results

1.10. DTI Tractography to obtain TMS targets

Within all subjects, probabilistic tractography from a BA25 seed (Figure 3) elucidated a clear and consistent pathway to ipsilateral cortex at a highly accessible scalp site. These group tractography data show ipsilateral connectivity to two targets in the medial frontal pole, one superior to the other by about 1 cm. The path to medial frontal pole (BA10) was judged the shortest to a TMS accessible site. All subjects showed similar ipsilateral connectivity between the BA25 seed area and the medial frontal pole as estimated by diffusion tractography. Thus, for each subject, the TMS stimulation site was chosen as the scalp location that was closest to the cortical site of strongest connectivity to the seeded BA25 region.

In addition to the tractography-derived stimulation sites, the actual TMS coil placement in the scanner prior to and after interleaved TMS–fMRI was obtained using fiducial markers, and served to provide a ground-truth estimate of the spatial location of targeting (notice that this degree of precision is often absent from most TMS applications because of the lack of general quantitative reporting). Because of individual variation in DTI-determined targets, the coil placement was slightly different for every subject (Figure 4). When transformed into standard space the group average location was $X = 12.9$ mm, $Y = 85.2$ mm, and $Z = 7.1$ mm, and the individual stimulation sites fell within a 5 cm diameter area on the forehead centered on those coordinates, with a mean distance from center of 10.1 ± 8.1 mm. Fiducial measures also confirmed that the difference in the site determined by DTI

and the site of coil placement at the beginning of the scan was less than 2 mm. Further, on average, as determined from the fiducial measures and from motion correction during functional analysis, head movement across scans was not greater than 2 mm in any direction for each of the ten subjects.

1.11. Whole-brain analysis of stimulation intensity

Both whole-brain and ROI analyses were performed for the contrasts of 100%, 120%, and 140% conditions with the 80% baseline; ROI analyses were performed at four locations: the deep target BA 25 and corresponding BA 25 in the contralateral (left) hemisphere, and the right hemisphere frontal pole region that contained the TMS stimulation site, and a dorsal prefrontal cortical site that did not show connectivity with the seeded region (Figure 2). Whole-brain results, summarized in Table 1, demonstrate a highly selective effect in right hemisphere BA 25 showed activation for both supra- threshold stimulation levels (120% and 140%) relative to 80%, though only the former survived cluster correction for multiple comparisons (z-score threshold $t > 2.78$ and cluster significance $p < 0.1$), showing an increase in activation in our BA25 centered region of interest (Figure 5A). This subgenual cluster of activated voxels encompassed the BA 25 gray matter bordering the starting point of the DTI tracing, centered on MNI coordinates of −6, 14, −6.

Outside of these a priori regions, activations at each stimulus intensity showed strong and diffuse activation patterns outside the tractography-generated regions of interest as well. Anecdotally, we observed strong auditory cortex activation and midbrain activation at all stimulation levels, but this is also obvious from the targeted contrasts in Figure 5. In contrast, the right hemisphere stimulation site showed a significant *decrease* in activation in the 140% - 80% contrast (Figure 5B). This deactivation was uncorrelated (across subjects) with the BA25 effect ($r = 0.06$) and therefore represent relatively independent phenomena. Nonetheless, this deactivation is interesting because it suggests that for studies interested in exciting cortical surface underneath the coil (arguably, the majority of TMS-fMRI studies), TMS intensity does not scale linearly with the BOLD response in the underlying cortex; more dose-response experiments are clearly needed. Nonetheless, our analysis was focused on subcortical BA25 activation, which we explore further below.

More targeted ROI-level results revealed the same pattern. As shown in Figure 6, increasing TMS intensity produced increased a significantly greater ($z = 1.65$, $p < 0.05$) number of activated voxels in both the left and right BA25 target ROIs. No significant activations were seen in the control ROI. A similar pattern can also be seen when BOLD activation in the four ROIs is plotted (Figure 6B): again, an increasing activation with TMS intensity is found in the target right BA25 ROI, activation in left BA25, although with no increase with TMS intensity, and deactivation with increasing intensity in the frontal pole stimulation site and frontal control site.

Additionally, to ensure that the effects observed were not attributable to individual differences in effective dose due to relative differences in scalp-to-cortex distance at M1 and the BA10 stimulation site, we calculated the difference in scalp-to-cortex distance (as estimated by the Euclidean distance between the site of stimulation and the nearest cortex surface) at each location. This linear scaling factor (across subjects mean difference =

1.34mm ± 2.97) was uncorrelated with both the delivered electric field (r = 0.39; p = 0.27) or the BOLD increase at the target BA25 site (Left BA25: r = 0.05, p = 0.89; Right BA25: r = 0.12, p = 0.74).

1.12. OrT covariance analysis

Beyond a group level analysis, we sought to confirm the stimulus intensity dependence of activation in our deep brain target within individual subjects. To achieve this, an OrT analysis was performed to test for a monotonically increasing activation resulting from stimulation at increasing (80%, 120%, and 140%) TMS intensities. The best-fit model leading to the lowest AIC value resulted from the combination of the first three principal components, in which 90% of the subjects showed monotonic increases in their subject scores associated with each intensity condition in this model (Figure 7). Permutation testing estimated a significant p-value for this model ($p < 0.03$).

The voxel pattern associated with the best-fit model, includes BA 25, and is displayed in Figure 8, and the estimated z-values from the bootstrapping procedure for the regions of greatest activation and deactivations are listed in Table 2. As can be seen in both the table and the figure, the deep target BA 25 site is significantly activated within the pattern; it should be emphasized here that there were no *a priori* spatial constraints on the data in this multivariate analysis, in other words, the emergence of BA25 activation and its increasing activation across TMS intensity condition emerged naturally from the whole brain data. Since the model thus reflects monotonic BA25 increases as TMS intensity increased, this result is in line with the findings in the whole brain and ROI analysis above, but demonstrates the increases of activation with TMS intensity on an individual basis (Figure 7). Also in line with the ROI findings, the right frontal pole stimulation site shows decreasing activation with increasing TMS intensity (see Figure 8, Table 2).

1.13. Seed-based functional connectivity validation

We evaluated the similarity of cortical targets suggested by seed-based functional connectivity and targets identified above via tractography. Group analyses revealed a strongly selective pattern of functional connectivity with the BA25 seed, limited to regions of the ventrolateral PFC and bilateral hippocampal cortex (Figure 9). However, these patterns are largely descriptive, as the effective use of fMRI connectivity was to find the individual's peak of activation within BA10 that was near (within 10mm or the cortical surface (see Methods); individual functional peak locations (i.e., targets) are visualized in Figure 10B. Next, we sought to evaluate to proximity of the actual site of stimulation to the target sites suggested by structural and functional connectivity. As out- lined above, reliable neuronavigation within the MR environment is challenging for many reasons; we were nonetheless able to correct for any error in coil placement and locate the precise site of stimulation using MR-sensitive fiducial markers. We evaluated the Euclidean distance between cortical stimulation sites suggested by either tractography-based or functional-connectivity-based targets and the actual site of stimulation. We compared this distance with the over- all stimulation effect (the slope of the increase in stimulation effect from the OrT described above), and found a significant negative association between the stimulation effect and the discrepancy distance for the functional ($r_{10} = -0.64$, $p < 0.05$), but not

structural targets (r_{10} = −0.16; Figure 10D). This result suggests that deviation from a the functional target decreases the degree of subgenual recruitment via deep-brain TMS. Subject-specific targets based on tractography information demonstrated a greater spatial precision (mean eccentricity: 5.2 ± 2.5) than targets derived from functional connectivity (mean eccentricity: 12.7 ±7.1), and therefore suggested a more consistent cortical tar- get for TMS. Nonetheless, this degree of spatial variation amongst individuals may nonetheless be an important predictor of treatment response, and suggests functional information should be incorporated in future applications of connectivity-based targeting.

Discussion

In the present study, we used a novel combination of fMRI- and DTI-based methods to find scalp targets to a seed region deep in the brain near BA 25. Both fMRI- and DTI-based connectivity from this region showed direct connections in all subjects with cortical targets in frontal pole cortex. Owing to their greater spatial precision, we used diffusion tractography-based targets as a basis for localizing stimulation within the MR scanner. Single pulses of TMS to these individualized frontal sites during fMRI recording significantly activated the deep targets. This activation increased with TMS intensity, providing evidence that the deep targets were directly activated transynaptically via TMS. The increasing activation in BA25 was demonstrated in two different measures using an ROI analysis, and also in a multivariate analysis of whole brain data. Existing technology for focal deep brain stimulation is invasive because it requires surgical implantation of electrodes and pulse generators. Existing techniques for noninvasive brain stimulation are focal but superficial (as in the case of conventional TMS), or they are deep but nonfocal (as in the case of TMS coils specialized for deeper brain stimulation, or transcranial electrical stimulation). The present results suggest a new technique for brain stimulation technology that has all three of the following features: it is (1) noninvasive, (2) target-specific and (3) deep, providing a means of studying brain-behavior relationships of neurocircuits that involve deep regions.

Three other studies have reported modulation of BA25 while employing interleaved TMS/fMRI (Dowdle et al., 2018; Oathes et al., 2018; Vink et al., 2018). While testing a within-scanner sham technique, Dowdle et al. (2018) reported that single TMS pulses to DLPFC resulted in activation of subcortical structures, including an anterior cingulate cortex (ACC) region that included BA25. While stimulating at four different intensity levels (90%, 100%, 110% and 120% of MT) similar to those used in the present study, they did not find any significant differences in activation between dose levels, while these were found here. Two factors may explain this difference: first, Dowdle et al. used a scalp-based targeting method (using the site F3 from the International 10/20 EEG System) rather than basing targeting on individualized brain imaging, as was done using DTI here, and second, DLPFC was stimulated, which may have more limited direct connectivity with BA25 than the frontal pole. Vink et al. (2018) also stimulated DLPFC, using two intensity levels (60% and 115% MT), and reported activation in BA25 when contrasting the two intensity levels, but only in four of the ten subjects. Here too, the use of TMS targeting method (an anatomical landmark on structural MRIs) rather than individualized connectivity measures, and targeting DLPFC rather than frontal pole, most likely led to differences with the present study. Oathes et al.

(2018) did use a resting state connectivity measure, again targeting DLPFC, but instead of modulating TMS intensity, employed an alternative strategy of using multiple spatial targets. They found a not quite significant decrease in BA25 activity with TMS. A fourth study using TMS/fMRI interleaving also stimulated DLPFC, using four TMS intensity levels (80%, 90%, 100% and 110% of MT), and using resting state connectivity to target with (Tik et al., 2017). They reported dose-dependent activation of an ACC region near BA25, although contrary to the present study, the activation decreases from 90% to 110%, with the latter showing deactivation, similar to that seen by Oathes et al. (2018). This difference in dosage dependency is again most likely attributable to the difference in connectivity of BA25 with DLPFC and with frontal pole, although the Tik et al. report was a published meeting abstract, and more details are needed for a useful comparison.

All of these studies have used DLPFC as a superficial stimulation site, and none have made use of DTI, which provides a more direct anatomical measure. Another group should be mentioned which has used frontal pole as a stimulation target to successfully activate a target subcortical structure in an interleaved TMS/fMRI study (Hanlon et al., 2013), although scalp-based targeting was used (electrode site FP1), only a single TMS intensity level was used, and the subcortical targets did not include BA25. The frontal pole stimulation did activate orbitofrontal cortex and ACC, although BA25 wasn't specifically differentiated. Overall, these interleaved TMS/fMRI studies all demonstrate in principle the use of network-connectivity based targeting of subcortical structures, which the present study has added DTI-based targeting and a significant TMS dosage dependency in the targeted subcortical activation.

4.1 Definition of superficial targets using neuroimaging

From its inception, the concurrent use of TMS and brain imaging has demonstrated that stimulation of superficial cortical targets can result in measurable effects at remote sites including those that are deep from the surface of the brain. For example, TMS to motor cortex, besides activating the stimulated region, also produced significant activation effects bilaterally in premotor cortex, in contralateral motor cortex, and in SMA, areas known to be directly connected to motor cortex. Motor cortex stimulation also produced responses in deeper regions as well, for example in the putamen, thalamus and cingulate cortex (Bestmann et al., 2004; Denslow et al., 2005). In general, inter- leaved TMS–fMRI studies demonstrate widespread effects of rTMS applied to deep cortical regions, including effects in orbitofrontal cortex, hippocampus, and other limbic regions. Furthermore, TMS-induced subcortical activity was found to be dependent upon the structural integrity of the white matter fiber tracts (Kearney-Ramos et al., 2018).

Increasingly, the capacity of TMS to affect regions remote from the point of stimulation has been exploited in TMS-fMRI studies examining connectivity and network function (e.g., Feredoes et al., 2011; Silvanto et al., 2006; Ruff et al., 2006, 2008, 2009). For example, in a series of studies (Ruff et al., 2006, 2008, 2009) it was shown that TMS to the frontal eye fields affected fMRI activation of occipital visual areas, along with perceptual function, in a topographic manner, and that these effects on visual cortex differed from those caused by TMS to intraparietal sulcus. The present study adds to the use of interleaved TMS-fMRI to

investigate brain network function by demonstrating the use of DTI to enable the targeting of TMS to BA25, a region inaccessible to direct TMS. Presumably, the technique used here can be generalized, guiding TMS to stimulate any brain region of interest, no matter its depth. Just as important, this targeting can be done on an individual basis. As has been shown previously, the use of imaging data to adjust targeting TMS using individual differences can have a dramatic effect on the potency of the stimulation (Sack et al., 2009), and that there can be large differences between individuals in where stimulation should be applied to influence deep targets (Fox et al., 2012). As illustrated in Figure 4, the location of TMS coil placement, determined by the end point of the individual DTI pathway, varied between subjects across a range of 5 cm. Targeting by group means would have meant that the point of greatest stimulation could have been off in some individuals by over 2 cm, dramatically reducing the effective stimulation over the actual area most directly connected in those individuals to white matter tracts revealed by DTI that were connected to the deep target.

Lastly, while the present analysis has focused on second-step connections to subcortical regions, access to subcortical targeting has motivated the development of TMS coils with deeper penetration than conventional coils that are limited to brain regions lying close to the surface (Levkovitz et al., 2007; Roth et al., 2007). These H-coil designs have shown promise and are now FDA approved for treatment of MDD and OCD. However, the drawback is that these coils only increase the electric field penetration depth up to 1 cm deeper compared to conventional figure-8 coils, and therefore not enough to induce a suprathreshold electric field in BA25 (Deng et al., 2013, 2014). While tantalizing in its simplicity, we nonetheless believe that the most promising approaches for DBS lie in a more fundamental understanding of structural and functional network properties of the stimulated cortex, as outlined in the current study.

1.14. Diffusion-based targeting for treatment of depression

Beyond increasing the ability to use combined brain imaging and stimulation to investigate brain function, the present results suggest that DTI-based TMS targeting can extend the effectiveness of TMS in therapeutic applications, allowing treatment of disorders with heavy involvement of brain regions too deep to be directly assessable by conventional TMS coils. Models of how cortical-subcortical connectivity could be used to guide rTMS treatment protocols fall generally under two models: a diagnostic model, and a more mechanistic cognitive neuroscience model. The diagnostic model uses patterns of functional activation to identify individualized targets, as discussed above. Such assessments are relatively quick (resting scans last ~10minus in an MRI), and their generalizability is broad. Alternatively, the cognitive neuroscience model of a trans-synaptic treatment protocol has been suggested by the work (e.g., Wang et al., 2014) in which repeated high frequency TMS trains were applied to superficial parietal cortex to affect a hippocampal memory network over repeated sessions to create a cumulative change (there, an increase in memory performance). Both of these approaches have value, and it is likely that the most efficacious protocols will be a healthy marriage between clinical and cognitive neuroscience principles (Luber et al., 2017). While the present study is only preliminary, and requires further work to optimize trans-synaptic modulation of a subcortical structure, such a model seems a reasonable first approach to developing a therapy.

In addition, available evidence demonstrates that more focused stimulation, for example by using imaging to guide TMS coil placement for superficial targets, improves outcomes, in both basic and clinical studies. Indeed, the effect of TMS on a cognitive task was greatest when targeted based upon individual fMRI task activation (Cohen's d=1.13), and this was superior to structural MRI-targeting (d=0.82), probabilistic targeting (d=0.67), or the 10–20 EEG system (d=0.34) (Sack et al., 2009). fMRI guidance of TMS on an individual basis has been successfully applied, for example in targeting auditory hallucinations in schizophrenia (Hoffman et al., 2007), or in the modulation of working memory circuits (Luber et al., 2008; Beynel et al., 2019). In TMS treatment of depression, MRI-guided stereotaxic coil placement (Fitzgerald et al., 2009; Rusjan et al., 2010) is beginning to be adopted, and has contributed to higher response rates than the standard targeting (Downar & Daskalakis, 2013). In the present study, we have extended this image-guided targeting approach beyond the refinement of superficial targeting to targeting in depth, informed by connectivity with deep brain structures, and furthermore we have verified target engagement using interleaved TMS–fMRI.

In adding the engagement and modification of deeper targets to the brain stimulation toolbox for possible use in treatment of psychiatric illnesses, its use in treating depression might be questioned. As noted in the Introduction, the DLPFC has limited direct connectivity with critical nodes in the depression neurocircuit based on tract-tracing studies in animals and DTI studies in humans (Price and Drevets, 2010; Gutman et al., 2009; Haber et al., 2006; Haber and McFarland, 1999). Yet stimulation of DLPFC has been shown to be efficacious in treating depression- suggesting that clinical improvement is driven by something other than anatomical connectivity between the cortical target and the network that needs to be modulated. A case can be made that the antidepressant effects of DLPFC stimulation may have to do with the modulation of cortical networks involved with emotional regulation, leading to indirect changes in deeper networks (e.g., Luber et al., 2017). However, as we discuss in the introduction, there is evidence that direct action (for example with DBS) on deeper structures can have a profound antidepressant effect, and, based on this, we suggested that one potential use of transsynaptic stimulation might be to directly target deeper structures and so directly modulate deeper networks involved with depression in a potentially more efficacious way.

It is also relevant to note that resting-state correlations between DLPFC and subgenual cortex are consistently negative (Fox et al., 2014; Fox et al., 2012). While an anticorrelation is in itself not a basis for therapeutic inference, this body of research proceeds on the sound justification that "the clinical effects of brain stimulation are related, if not dictated, by the connectivity of the target site" (Cash et al., 2021a). This pattern has been further interpreted to suggest that TMS to a targeted, anticorrelated DLPFC region is effective because it takes advantage of this anticorrelated pattern, and exaggerates it, possibly dampening the subgenual response (Cash et al., 2021b). Nonetheless, such a mechanistic interpretation is largely speculative, and will remain so without reliable concurrent stimulation and neuroimaging information (e.g., TMS-fMRI) that affords the ability to directly assess the effects of stimulation on BOLD activity and connectivity.

The relationship between functional connectivity in the BA10 stimulation sites and subgenual cortex (BA25) was consistently *positive* in our resting state analyses, in contrast to the negative relationship between DLPFC and BA25. While it is difficult to draw lasting implications of this relationship, this finding points to a larger gap in our understanding of *why* such connectivities predict treatment efficacy. We believe that any reliable conjecture on the putative mechanism of (either positive or negative) correlations between stimulation and target sites, (with either BA10 or DLPFC stimulation sites, respectively), and their outcomes for therapeutic intervention would rely on two principle characteristics: a) a reliable characterization of the cognitive functions subsumed by the stimulation site, and b) a thorough using both resting state and task related fMRI (preferably using emotionally relevant tasks). This is no small challenge, as both BA10 and DLPFC are highly multimodal regions which are responsible for a wide array of cognitive functions (Davis and Cabeza, 2015; Kievit et al., 2014) and thus difficult to characterize. Thus, as targets for therapy continue to evolve and develop in light of their clinical efficacy, it is also critical that the theoretical explanations for the effective selection of such targets continues apace.

1.15. Specificity of targeting in TMS-fMRI

While the phrase “target-specific” was used to describe the use of the tractography-guided technique to activate BA25, the “specific” aspect deserves some qualification. As described above, a TMS pulse not only affects the brain beneath the coil to a depth determined by the effective electric field it produces (Figure 1), but other regions the stimulated area is connected to. This can be seen in the present study in the other areas significantly activated and listed in Table 1, with, for example, activations in medial PFC and insular cortex which are likely due to direct connections with the frontal pole (Liu et al., 2013). Besides regions directly connected with the stimulated region, the TMS pulse causes a number of other effects in the brain: for example, activations in auditory (temporal) cortex due to the clicking of the TMS coil, in somatosensory cortex due to stimulation of sensory nerves in the scalp by the electric field and vibration of the coil, and in midbrain, due to stimulation of the trigeminal nerve and to the startle reflex, while activations in insula, brainstem, and dorsal anterior cingulate cortex may have occurred due to pain responses (Table 1). However, in the present study focal targeting was meant to denote the capacity to intentionally activate a deep target transynaptically via TMS based on DTI from a seed in that target, and to do so in a dosage-dependent manner, as was successfully achieved with BA 25. Furthermore, cortical targets suggested by diffusion tractography were more spatially precise (lower eccentricity across participants) than targets suggested by resting-state functional connectivity. Cortical sites based on white matter anatomy generally have a greater generalizability across subject populations, and are likely to be more reliable than connectivity-based methods of establishing functional networks within subjects (Bennett & Miller, 2010). Nonetheless, besides activating the intended target region, it is important to keep in mind that TMS clearly activates other anatomically and functionally related regions as well, and that activation of other regions can also contribute to TMS-induced effects. Future improvements in coil design to reduce ancillary stimulation effects like acoustic noise would be useful in lowering some of these confounding effects.

In addition to questions of focality, another aspect of targeted TMS is how direct the stimulation was. The simplest reason a region that is closely connected to a stimulated area might show activation is that it is responding to a volley of action potentials due to the stimulation. However, an area functionally related to the stimulated region can show imaging changes in activation without being directly stimulated in this sense. For example, subthreshold TMS to motor cortex, which is not expected to directly generate action potentials in cell axons, typically results in activations of directly connected motor areas such as ipsilateral premotor cortex and SMA (Bestmann et al., 2003; Fox et al., 2006; Hanakawa et al., 2009; Speer et al., 2003). Even with transcranial direct current stimulation, remote activation of ventral midbrain regions has been found with prefrontal cortex stimulation (Chib et al., 2013). Clearly, modulation of activity with brain stimulation in one part of a distributed network can affect other closely-connected regions without volleys of action potentials caused by stimulation, for example through compensatory shifts in the balance of activity (Lomber et al., 1999). In the present study, the response of BA 25 was measured as the intensity of TMS to the frontal pole was parametrically varied across four levels, from well below motor threshold (and assumed to be below excitability threshold in frontal pole) to three higher supra-MT levels that might be expected to generate increasingly larger volleys of action potentials to the monosynaptically connected BA25. A previous study used single pulses of TMS and looked at the fMRI response of directly connected brain regions to two levels of intensity, above and below motor threshold, finding increased activation with intensity (Shitara et al., 2011). Across the four intensity levels of the present study, TMS dosage dependency of activation in BA25 was demonstrated in two ways. First, percent volume of significantly activated voxels increased monotonically with TMS intensity (Figure 7). Second, ordinal trends covariance analysis produced a network whose activation was significantly related to increasing TMS dosage, with BA 25 being one of the most significant nodes of that network. While we conclude that our dosage effects on BA25 activation were a result of its direct anatomical connectivity with the stimulated frontal pole, further development of this method should compare the effects of anatomical and functional connectivity on subcortical target engagement.

1.16. Diffusion- versus functionally-based targeting

A secondary goal of this analysis was to determine the efficacy of tractography-based targeting compared to functionally-based targeting for deep-brain targets in TMS. A number of previous studies have demonstrated that functionally based targeting, based on resting state correlations with a deep-brain seed region, provide meaningful targets for neuromodulation which may predict treatment response (Cash et al., 2019; Fox et al., 2012; Wang et al., 2014). The logic of this method of targeting is based on the idea that nodes within a consistently activated cortical network should demonstrate resonance within that network when receiving an outside stimulus. It is relevant to note that resting-state correlations between DLPFC and subgenual cortex are consistently negative (Fox et al., 2012c). While an anticorrelation is in itself not a basis for therapeutic inference, this body of research proceeds on the sound justification that “the clinical effects of brain stimulation are related, if not dictated, by the connectivity of the target site” (Cash et al., 2021). This pattern has been further interpreted to suggest that TMS to a targeted, anticorrelated DLPFC region is effective because it takes advantage of this anticorrelated pattern, and

exaggerates it, possibly dampening the subgenual response (Cash et al., 2021). Nonetheless, such a mechanistic interpretation is largely speculative, and will remain so without reliable concurrent stimulation and neuroimaging information (e.g., TMS-fMRI) that affords the ability to directly assess the effects of stimulation on BOLD activity and connectivity.

Cortical targets based on DTI, in contrast, follow a similar but complimentary logic, though the basis for activation is anatomical, not functional. The current analysis is the first to explore which method should provide greater efficacy in stimulating a deep-brain target. We found that, as might be expected from an anatomical target, DTI-based target locations were more tightly clustered than functional targets. At a group level, structurally-defined targets resulted in more spatially homogenous pattern of cortical targets (Figure 10A) than functionally-based cortical targets (Figure 10B), which had greater eccentricity in our population. This different could be due to many factors, but mostly likely due to the fact that white matter anatomy, at a gross scale, is highly conserved across individuals. Nevertheless, more explicit comparisons of these alternative techniques is necessary. The advance of electric field modeling techniques (e.g., Figure 1) have shown that even small changes in coil positioning and orientation have clear impacts on treatment response (Caufield et al., 2021). Nonetheless, the efficacy of a particular targeting technique is likely to benefit from more consistent cortical positioning across subjects, as greater eccentricity to a standard targeting location is likely to introduce errors in positioning across individuals. To this end, we next evaluated the extent to which this eccentricity was functionally meaningful. As depicted in Figure 10D, we found that a greater stimulation effect was associated with a smaller distance between the stimulation site and the cortical target suggested by functional connectivity. A similar relationship was not present for cortical targets suggested by tractography methods; this null relationship might be due to restricted range explainable by the DTI based targeting approach. This result suggests that the greater eccentricity introduced by functional targeting techniques may introduce a consistent confound in potential treatment efficacy. Nonetheless, the present data are underpowered and suggest that a combination of diffusion-based and functional-connectivity-based information are still necessary for optimum target placement. Nonetheless, given the evidence for dosage-dependent activation of BA 25 related to frontal pole stimulation one synapse away, we conclude that DTI-guided TMS of superficial cortex did indeed directly activate a selected deep target beyond the immediate influence of the effective electric field. Further, the dosage-dependent response in BA25 suggests a mechanism for titration of deep target modulation in potential therapeutic applications of noninvasive brain stimulation.

Lastly, another possibly relevant finding related to the parametric manipulation of TMS intensity was that the activation of the stimulated frontal pole cortex decreased with increasing intensity (Figures 7 and S3). Previous use of single TMS pulses in interleaved TMS/fMRI has been minimal (Bestmann et al., 2003; Bohning et al., 2000; Hanakawa et al., 2009; Shitara et al., 2011): most studies using the technique employ bursts of rTMS in trains lasting from about 0.5–20 s (Siebner et al., 2009). The previous single pulse studies were performed over motor cortex. All found a small activation for supra-MT intensity pulses. However, this activation may be confounded with afferent signals resulting from the TMS-caused muscle twitch (Bestmann et al., 2003). Shitara et al. (2011) found anomalies in the hemodynamic response function in the cortex regions under the coil due to the TMS

pulse, and suggested this might result in lowered measured activation. They also raised the possibility that lowered activation could be due to suppression of neural activity following the initial excitation caused by the pulse. It has long been known that TMS to motor cortex produces a silent period in EMG occurring after the initial muscle twitch, and that the duration of this silent period is proportional to the intensity used, and this has been attributed to a corresponding silent period in motor cortex activity. A prolonged silent period in neural activity after an initial burst due to TMS has also been observed in single cell recordings in cats (Allen et al., 2007). Following Shitara et al. (2011), these lead to the suggestion that the activation at the stimulation site which decreased with increasing TMS intensity may be related to a period of relative inactivity in the stimulated area caused by the TMS pulse and which increases in duration with intensity. On the other hand, a more recent study found TMS dose-dependent activation beneath the stimulating coil in motor cortex using a newly-developed multichannel receive MR coil in place of the standard birdcage coil, suggesting activation directly beneath the TMS coil can be detected with a more sensitive MRI system (Navarro de Lara et al., 2017).

1.17. Conclusion

In the present study DTI tractography beginning in a brain region too deep for effective direct TMS was used to find a superficial cortical site one synapse away which could be effectively stimulated. Then using interleaved TMS-fMRI, it was demonstrated that DTI-guided TMS could activate the deep target, and could do so in a dosage dependent manner, thereby demonstrating target engagement. The study has limitations that should be mentioned. It was performed as an initial proof-of-concept, with only a small sample of twelve healthy volunteers. Further studies should use a larger sample size. Moreover, while post hoc imaging analysis supported the engagement of the deep target with TMS stimulation of the superficial site, a more conclusive study should make use of multiple stimulation sites, some connected with the deep target, some not. When sham capability is added to fMRI-compatible coils, a sham condition should also be included in order to more directly account for activations caused by peripheral stimulation caused by the TMS coil. While the parametric use of TMS intensities somewhat obviates these limitations, without a control stimulation site or sham condition, non-specific TMS effects cannot be ruled out.

As to the relationship between anticorrelations assessed with functional data and DTI, unfortunately not much can be said. The field is growing to appreciate that functional and structural connectivity are only weakly correlated (Suarez et al., 2020), and that more one-to-one predictions are more likely in primary sensory/motor regions, rather than the complex association regions investigated in the current study. Nonetheless, it is an open question as to how structural pathways guide the functional response to cortical TMS, and the future applications of a confluence of technological, analytic, and theoretical tools opens fundamentally new opportunities in mapping this relationship.

Overall, however, this preliminary use of DTI-guided TMS suggests a new tool to extend the utility of non-invasive stimulation, enabling researchers to target deeper brain areas which previously were thought beyond reach. Here, the deep target was BA 25, which is hypothesized to be a key node in the neurocircuitry of depression. The successful activation

of BA 25 in a dosage-dependent manner suggests an initial step towards using DTI-guided TMS to noninvasively target areas for therapy no matter where they are situated in the brain.

Acknowledgements

This research was supported by a grant from NARSAD. B. Luber, Z.-D. Deng, and S. H. Lisanby are supported by the NIMH Intramural Research Program (ZIAMH00295). The work was done while they were at Duke University, prior to their NIMH employment. S.W. Davis was supported by National Institute of Aging Grant K01AG053539 and R21AG058161.

Disclosures

Z.-D. Deng and S. H. Lisanby are inventors on patents, patent applications on TMS technology assigned to Columbia University. A. V. Peterchev is inventor on patents, patent applications, and invention disclosures on TMS technology assigned to Columbia University and Duke University; he has received research support, patent royalties, and travel support from Rogue Research for cTMS technology licensed to them, travel support from Tal Medical, as well as a TMS equipment loan from MagVenture; he is supported by NIH (R01MH091083, R01NS088674), Duke Institute for Brain Sciences, and Duke University Energy Initiative.

References

Allen EA, Pasley BN, Duong T, & Freeman RD (2007). Transcranial magnetic stimulation elicits coupled neural and hemodynamic consequences. Science, 317, 1918–21. doi:10.1126/science.1146426. [PubMed: 17901333]

Baudewig J, Siebner HR, Bestmann S, Tergau F, Tings T, Paulus W, Frahm J (2001) Functional MRI of cortical activations induced by transcranial magnetic stimulation (TMS). Neuroreport 12:3543–3548. [PubMed: 11733708]

Bennett CM and Miller MB (2010) How reliable are the results from functional magnetic resonance imaging? Ann. N.Y. Acad. Sci 1191: 133–155, doi: 10.1111/j.1749-6632.2010.05446.x. [PubMed: 20392279]

Bestmann S, Baudewig J, Siebner HR, Rothwell JC, Frahm J (2003) Subthreshold high-frequency TMS of human primary motor cortex modulates interconnected frontal motor areas as detected by interleaved fMRI-TMS. Neuroimage 20:1685–1696. doi:10.1016/j.neuroimage.2003.07.028. [PubMed: 14642478]

Bestmann S, Baudewig J, Siebner HR, Rothwell JC, Frahm J (2004) Functional MRI of the immediate impact of transcranial magnetic stimulation on cortical and subcortical motor circuits. Eur J Neurosci 19:1950–1962. doi:10.1111/j.1460-9568.2004.03277.x. [PubMed: 15078569]

Beynel L, Davis SW, Crowell CA, Hilbig SA, Lim W, Nguyen D, Palmer H, Brito A, Peterchev AV, Luber B, Lisanby SH, Cabeza R, & Appelbaum LG (2019). Online repetitive transcranial magnetic stimulation during working memory in younger and older adults: A randomized within-subject comparison. PLoS One, 14, e0213707. doi:10.1371/journal.pone.0213707. [PubMed: 30901345]

Bien N, Roebroeck A, (2009) The brain's intention to imitate: the neurobiology of intentional versus automatic imitation. Cereb. Cortex, 19, 2338–2351. doi:10.1093/cercor/bhn251. [PubMed: 19153108]

Bohning DE, et al. , (1998) Echoplanar BOLD fMRI of brain activation induced by concurrent transcranial magnetic stimulation. Invest Radiol, 33(6): 336–40. [PubMed: 9647445]

Bohning DE, Shastri A, Wassermann EM, Ziemann U, Lorberbaum JP, Nahas Z, Lomarev MP, George MS (2000) BOLD-f MRI response to single-pulse transcranial magnetic stimulation (TMS). J Magn Reson Imaging 11:569–574. doi:10.1002/1522-2586(200006)11:6\<569::AID-JMRI1\>3.0.CO;2-3. [PubMed: 10862054]

Carpenter LL, Janicak PG, Aaronson ST, Boyadjis T, Brock DG, Cook IA, Dunner DL, Lanocha K, Solvason HB, & Demitrack MA (2012). Transcranial magnetic stimulation (TMS) for major depression: a multisite, naturalistic, observational study of acute treatment outcomes in clinical practice. Depress Anxiety, 29, 587–96. doi:10.1002/da.21969. [PubMed: 22689344]

Cash RFH, Cocchi L, Lv J, Fitzgerald PB, Zalesky A (2021a) Functional Magnetic Resonance Imaging-Guided Personalization of Transcranial Magnetic Stimulation Treatment for Depression. JAMA Psychiatry 78, 337–339. [PubMed: 33237320]

Cash RFH, Cocchi L, Lv J, Wu Y, Fitzgerald PB, Zalesky A (2021b) Personalized connectivity-guided DLPFC-TMS for depression: Advancing computational feasibility, precision and reproducibility. Hum Brain Mapp.

Cash RFH, Zalesky A, Thomson RH, Tian Y, Cocchi L, Fitzgerald PB (2019) Subgenual Functional Connectivity Predicts Antidepressant Treatment Response to Transcranial Magnetic Stimulation: Independent Validation and Evaluation of Personalization. Biol Psychiatry.

Caufield KA, Li X, and George MS (2021) Four electric field modeling methods of dosing prefrontal transcranial magnetic stimulation (TMS): Introducing APEX MT dosimetry. Brain Stimulation, 14: 1032–1034. [PubMed: 34186248]

Chib VS, Yun K, Takahashi H, Shimojo S (2013) Nonivasive remote activation of the ventral midbrain by transcranial direct current stimulation of prefrontal cortex. Translational Psychiatry, 3, e268; doi:10.1038/tp.2013.44. [PubMed: 23756377]

Cho SS and Strafella AP (2009) rTMS of the left dorsolateral prefrontal cortex modulates dopamine release in the ipsilateral anterior cingulate cortex and orbitofrontal cortex. PLoS One, 4(8): e6725. doi:10.1371/journal.pone.0006725. [PubMed: 19696930]

Davis SW, Cabeza R, 2015. Cross-hemispheric collaboration and segregation associated with task difficulty as revealed by structural and functional connectivity. J Neurosci 35, 8191–8200. [PubMed: 26019335]

Davis SW, Luber B, Murphy DLK, Lisanby SH, Cabeza R, (2017). Frequency-specific neuromodulation of local and distant connectivity in aging and episodic memory function. Hum Brain Mapp 38, 5987–6004. [PubMed: 28885757]

Deng Z-D, Lisanby SH, and Peterchev AV (2011) Electric field strength and focality in electroconvulsive therapy and magnetic seizure therapy: a finite element simulation study, J Neural Eng, 8: 016007. doi:10.1088/1741-2560/8/1/016007. [PubMed: 21248385]

Deng Z-D, Lisanby SH, and Peterchev AV (2013) Electric field depth–focality tradeoff in transcranial magnetic stimulation: simulation comparison of 50 coil designs. Brain Stimul, 6: 1–13. doi:10.1016/j.brs.2012.02.005. [PubMed: 22483681]

Deng ZD, Lisanby SH and Peterchev AV (2014). Coil design considerations for deep transcranial magnetic stimulation. Clin Neurophysiol 125: 1202–1212. doi:10.1016/j.clinph.2013.11.038. [PubMed: 24411523]

Deng ZD, Liston C, Gunning FM, Dubin MJ, Fridgeirsson EA, Lilien J, van Wingen G, and van Wararde J (2018) Electric field modeling for transcranial magnetic stimulation and electroconlusive therapy. In Brain and Human Body Modeling: Computational Human Modeling at EMBC 2018.

Denslow S, et al. , (2005) Cortical and subcortical brain effects of transcranial magnetic stimulation (TMS)-induced movement: an interleaved TMS/functional magnetic resonance imaging study. Biol Psychiatry, 57(7): 752–60. doi:10.1016/j.biopsych.2004.12.017. [PubMed: 15820232]

Dougherty DD (2018). Deep brain stimulation: clinical applications. Psychiatr Clin North Am, 41, 385–94. doi:10.1016/j.psc.2018.04.004. [PubMed: 30098652]

Dowdle LT, Brown TR, George MS, & Hanlon CA (2018). Single pulse TMS to the DLPFC, compared to a matched sham control, induces a direct, causal increase in caudate, cingulate, and thalamic BOLD signal. Brain Stimul, 11, 789–96. doi:10.1016/j.brs.2018.02.014. [PubMed: 29530447]

Downar J, & Daskalakis ZJ (2013). New targets for rTMS in depression: a review of convergent evidence. Brain Stimul, 6, 231–40. doi:10.1016/j.brs.2012.08.006. [PubMed: 22975030]

Feredoes E, Heinen K, Weiskopf N, Ruff C, and Driver J (2011) Causal evidence for frontal involvement in memory target maintenance by posterior brain areas during distracter interference of visual working memory. Proc Nat Acad Sci, 108: 17510–17515. doi:10.1073/pnas.1106439108. [PubMed: 21987824]

Ferrarelli F, Haraldsson HM, et al. (2004) A [17F]-fluoromethane PET/TMS study of effective connectivity. Brain Res. Bull. 64 (2), 103–113. doi:10.1016/j.brainresbull.2004.04.020. [PubMed: 15342097]

Fitzgerald PB, Hoy K, McQueen S, et al. (2009) A randomized trial of rTMS targeted with MRI based neuro-navigation in treatment-resistant depression. Neuropsychopharmacology 34 (5), 1255–1262. doi:10.1038/npp.2008.233. [PubMed: 19145228]

Fonzo GA, Goodkind MS, Oathes DJ, Zaiko YV, Harvey M, Peng KK, Weiss ME, Thompson AL, Zack SE, Lindley SE, Arnow BA, Jo B, Gross JJ, Rothbaum BO, & Etkin A (2017). PTSD psychotherapy outcome predicted by brain activation during emotional reac- tivity and regulation. Am J Psychiatry, 174, 1163–74. doi:10.1176/appi.ajp.2017.16091072. [PubMed: 28715908]

Fox P, Ingham R, George MS, Mayberg H, Ingham J, Roby J, Martin C, Jerabek P (1997) Imaging human intra-cerebral connectivity by PET during TMS. Neuroreport 8:2787–2791 [PubMed: 9295118]

Fox MD, Liu H, and Pascual-Leone A (2012a) Identification of reproducible individualized targets for treatment of depression with TMS based on intrinsic connectivity. NeuroImage, 66C: 151–160. doi:10.1016/j.neuroimage.2012.10.082.

Fox MD, Halko MA, Eldaief MC, and Pascual-Leone A (2012b) Measuring and manipulating brain connectivity with resting state functional connectivity magnetic resonance imaging (fcMRI) and transcranial magnetic stimulation (TMS). NeuroImage, 62, 2232–2243. 2232–43. doi:10.1016/j.neuroimage.2012.03.035. [PubMed: 22465297]

Fox MD, Buckner RL, Liu H, Chakravarty MM, Lozano AM, Pascual-Leone A (2014) Resting-state networks link invasive and noninvasive brain stimulation across diverse psychiatric and neurological diseases. Proc Natl Acad Sci U S A 111, E4367–4375. [PubMed: 25267639]

Fox MD, Buckner RL, White MP, Greicius MD, Pascual-Leone A (2012c) Efficacy of transcranial magnetic stimulation targets for depression is related to intrinsic functional connectivity with the subgenual cingulate. Biol Psychiatry 72, 595–603. [PubMed: 22658708]

George MS, Lisanby SH, Avery D, McDonald WM, Durkalski V, Pavli cova M, Anderson B, Nahas Z, Bulow P, Zarkowski P, Holtzheimer PE 3rd, Schwartz T, & Sackeim HA (2010). Daily left prefrontal transcranial magnetic stimulation therapy for major depressive disorder: a sham-controlled randomized trial. Arch Gen Psychiatry, 67, 507–16. [PubMed: 20439832]

de Graaf TA, Jacobs C, Roebroeck A, & Sack AT (2009). FMRIeffective connectivity and TMS chronometry: complementary accounts of causality in the visuospatial judgment network. PLoS One, 4, e8307. doi:10.1371/journal.pone.0008307. [PubMed: 20011541]

Greenberg BD, et al. , (2006) Three-year outcomes in deep brain stimulation for highly resistant obsessive-compulsive disorder. Neuropsychopharmacology, 31(11): 2384–93. doi:10.1038/sj.npp.1301165. [PubMed: 16855529]

Gutman DA, et al. , (2009) A tractography analysis of two deep brain stimulation white matter targets for depression. Biol Psychiatry, 65(4): 276–82. doi:10.1016/j.biopsych.2008.09.021. [PubMed: 19013554]

Habeck C, Krakauer JW, Ghez C, Sackeim HA, Eidelberg D, Stern Y, Moeller JR. (2005) A new approach to spatial covariance modeling of functional brain imaging data: ordinal trends analysis. Neural Computation. 17:1602−-1645. doi:10.1162/0899766053723023. [PubMed: 15901409]

Haber SN and McFarland NR (1999) Advancing from the ventral striatum to the extended amygdala: implications for neuropsychiatry and drug abuse. Annals of the New York Academy of Sciences, 877: 33–48. doi:10.1111/j.1749-6632.1999.tb09259.x. [PubMed: 10415641]

Haber SN, et al. , (2006) Reward-related cortical inputs define a large striatal region in primates that interface with associative cortical connections, providing a substrate for incentive-based learning. J Neurosci, 26(32): 8368–76. doi:10.1523/JNEUROSCI.0271-06.2006. [PubMed: 16899732]

Hadas I, Sun Y, Lioumis P, Zomorrodi R, Jones B, Voineskos D, Dow- nar J, Fitzgerald PB, Blumberger DM, & Daskalakis ZJ (2019). Association of repetitive transcranial magnetic stimulation treatment with subgenual cingulate hyperactivity in patients with major depressive disorder: a secondary analysis of a randomized clinical trial. JAMA Netw Open, 2, e195578. [PubMed: 31167023]

Hamani C Mayberg H Snyder B Giacobbe P Kennedy S Lozano AM. (2009) n stimulation of the subcallosal cingulate gyrus for depression: anatomical location of active contacts in clinical responders and a suggested guideline for targeting. Journal of Neurosurgery. 111(6):1209–1215. doi:10.3171/2008.10.JNS08763. [PubMed: 19480538]

Hanakawa T, Mima T, Matsumoto R, Abe M, Inouchi M, Urayama S, Anami K, Honda M, & Fukuyama H (2009). Stimulus-response profile during single-pulse transcranial magnetic stimulation to the primary motor cortex. Cereb Cortex, 19, 2605–15. doi:10.1093/cercor/bhp013. [PubMed: 19234068]

Hanlon CA, Dowdle LT, Correia B, Mithoefer O, Kearney-Ramos T, Lench D, Griffin M, Anton RF, and George MS (2013) Left frontal pole theta burst stimulation decreases orbitofrontal and insula activity in cocaine users and alcohol users. Drug and Alcohol Dependence; 178: 310–317. doi:10.1016/j.drugalcdep.2017.03.039.

Hannula H, Neuvonen T, et al. , (2010) Increasing top-down suppression from prefrontal cortex facilitates tactile working memory. Neuroimage 49, 1091–1098. doi:10.1016/j.neuroimage.2009.07.049. [PubMed: 19643184]

Hoffman RE, et al. , (2007) Probing the pathophysiology of auditory/verbal hallucinations by combining functional magnetic resonance imaging and transcranial magnetic stimulation. Cereb Cortex, 17(11): 2733–43. doi:10.1093/cercor/bhl183. [PubMed: 17298962]

Ilmoniemi RJ, Virtanen J, Ruohonen J, et al. , (1997) Neuronal responses to magnetic stimulation reveal cortical reactivity and connectivity. Neuroreport, 8:3537–3540. [PubMed: 9427322]

Johansen-Berg H, et al. , (2008) Anatomical connectivity of the subgenual cingulate region targeted with deep brain stimulation for treatment-resistant depression. Cereb Cortex, 18(6): 1374– 1383. doi:10.1093/cercor/bhm167. [PubMed: 17928332]

Kearney-Ramos TE, Lench DH, Hoffman M, Correia B, Dowdle LT, & Hanlon CA (2018). Gray and white matter integrity influence TMS signal propagation: a multimodal evaluation in cocaine-dependentindividuals. Sci Rep, 8, 3253. doi:10.1038/s41598-018-21634-0. [PubMed: 29459743]

Kievit RA, Davis SW, Mitchell DJ, Taylor JR, Duncan J, Cam CANRT, Henson RN, Cam CANRT (2014) Distinct aspects of frontal lobe structure mediate age-related differences in fluid intelligence and multitasking. Nat Commun 5, 5658. [PubMed: 25519467]

Kringelbach ML, Jenkinson N, Owen SL, & Aziz TZ (2007). Trans- lational principles of deep brain stimulation. Nat Rev Neurosci, 8, 623–35. doi:10.1038/nrn2196. [PubMed: 17637800]

Levkovitz Y, et al. , (2007) A randomized controlled feasibility and safety study of deep transcranial magnetic stimulation. Clin Neurophysiol, 118(12): 2730–2744. doi:10.1016/j.clinph.2007.09.061. [PubMed: 17977787]

Li X, Nahas Z, et al. (2004) Acute left prefrontal transcranial magnetic stimulation in depressed patients is associated with immediately increased activity in prefrontal cortical as well as subcortical regions. Biol. Psychiatry 55, 882–890. doi:10.1016/j.biopsych.2004.01.017. [PubMed: 15110731]

Liu H, Qin W/. Li W, Fan L, Wang J, Jiang T, and Yu C (2013) Connectivity-based parcellation of the human frontal pole with diffusion tensor imaging. J. Neurosci, 33: 6782–6790. doi:10.1523/JNEUROSCI.4882-12.2013. [PubMed: 23595737]

Lomber SG. (1999) The advantages and limitations of permanent or reversible deactivation techniques in the assessment of neural function. Journal of Neuroscience Methods, 86: 109–117. doi:10.1016/S0165-0270(98)00160-5. [PubMed: 10065980]

Luber B, Stanford AD, Bulow P, Nguyen T, Rakitin BC, Habeck C, Basner R, Stern Y and Lisanby SH (2008) Remediation of sleep-deprivation induced visual working memory impairment with fMRI-guided Transcranial Magnetic Stimulation. Cerebral Cortex 18 (9): 2077–2085. [PubMed: 18203694]

Luber B, Davis S, Bernhardt E, Neacsiu A, Kwapil L, Strauman TJ, and Lisanby SH (2017) Using neuroimaging to individualize TMS treatment for depression: Toward a new paradigm for imaging-guided intervention. NeuroImage, 148: 1–7; reprinted: NeuroImage, 151: 65–71; 10.1016/j.neuroimage.2016.12.083 [PubMed: 28062252]

Luber B, Stanford AD, Bulow P, Nguyen T, Rakitin BC, Habeck C, Basner R, Stern Y and Lisanby SH (2008) Remediation of sleep-deprivation induced visual working memory impairment with

fMRI-guided Transcranial Magnetic Stimulation. Cerebral Cortex 18 (9): 2077–2085. doi:10.1093/cercor/bhm231. [PubMed: 18203694]

Malone DA Jr., Dougherty DD, Rezai AR, Carpenter LL, Friehs GM, Eskandar EN, Rauch SL, Rasmussen SA, Machado AG, Kubu CS, Tyrka AR, Price LH, Stypulkowski PH, Giftakis JE, Rise MT, Malloy PF, Salloway SP, & Greenberg BD (2009) Deep brain stimulation of the ventral capsule/ventral striatum for treatment-resistant depression. Biol Psychiatry, 65(4): 267–275. doi:10.1016/j.biopsych.2008.08.029. [PubMed: 18842257]

Mayberg HS, Lozano AM, Voon V, McNeely HE, Seminowicz D, Hamani C, et al. , "Deep brain stimulation for treatment-resistant depression," Neuron, vol. 45, pp. 651–660, 2005. doi:10.1016/j.neuron.2005.02.014. [PubMed: 15748841]

Mian MK, Campos M, Sheth SA, & Eskandar EN (2010). Deep brain stimulation for obsessive-compulsive disorder: past, present, and future. Neurosurg Focus, 29, E10. doi:10.3171/2010.4.FOCUS10107.

Moeller JR, Habeck C (2006) Reciprocal benefits of mass-univariate and multivariate modeling in brain mapping: Applications to event-related functional MRI, H2 15O-, and FDG-PET. International Journal of Biomedical Imaging article ID 79862, doi:10.1155/IJBI/2006/79862.

Navarro de Lara LI, Tik M, Woletz M, Frass-Kriegl R, Moser E, Laistler E, and Windischberger C (2017) High sensitivity TMS/fMRI of the human motor cortex using a dedicated multichannel MR coil. NeuroImage, 150: 262–269. [PubMed: 28254457]

Oathes DJ, Zimmerman J, Duprat R, Cavdaroglu S, Scully M, Rosen- berg B, Flounders MW, Long H, Elliott M, Shandler G, Shino- hara RT, & Linn KA (2018). Individualized non-invasive brain stimulation engages the subgenual anterior cingulate and amygdala. bioRxiv, . doi:10.1101/503441.

O'Reardon JP, Solvason HB, Janicak PG, Sampson S, Isenberg KE, Nahas Z, Macdonald WM, Avery D, Fitzgerald PB, Loo C, Demi- track MA, George MS, & Sackeim HA (2007) Efficacy and safety of transcranial magnetic stimulation in the acute treatment of major depression: a multisite randomized controlled trial. Biol Psychiatry, 62(11): 1208–1216. doi:10.1016/j.biopsych.2007.01.018. [PubMed: 17573044]

Price JL and Drevets WC (2010) Neurocircuitry of mood disorders. Neuropsychopharmacology, 35(1): 192–216. doi:10.1038/npp.2009.104. [PubMed: 19693001]

Roberts DR, Vincent DJ, Speer AM, Bohning DE, Cure J, Young J, George MS (1997) Multi-modality mapping of motor cortex: comparing echoplanar BOLD fMRI and transcranial magnetic stimulation. Short communication. J Neural Transm 104:833–843. doi:10.1007/BF01285552. [PubMed: 9451716]

Roth Y, et al. , (2007) Three-dimensional distribution of the electric field induced in the brain by transcranial magnetic stimulation using figure-8 and deep H-coils. J Clin Neurophysiol, 24(1): 31–8. doi:10.1097/WNP.0b013e31802fa393. [PubMed: 17277575]

Ruff CC, Bestmann S, Blankenburg F, Bjoertomt O, Josephs O, Weiskopf N, et al. (2008) Distinct causal influences of parietal versus frontal areas on human visual cortex: evidence fromnconcurrent TMS–fMRI. Cerebral Cortex, 18: 817–827. doi:10.1093/cercor/bhm128. [PubMed: 17652468]

Ruff CC, Blankenburg F, Bjoertomt O, Bestmann S, Freeman E, Haynes JD, et al. (2006) Concurrent TMS–fMRI and psychophysics reveal frontal influences on human retinotopic visual cortex. Current Biology, 16: 1479–1488. doi:10.1016/j.cub.2006.06.057. [PubMed: 16890523]

Ruff CC, Blankenburg F, Bjoertomt O, Bestmann S, Weiskopf N, and Driver J. (2009) Hemispheric differences in frontal and parietal influences on human occipital cortex: direct confirmation with concurrent TMS–fMRI. Journal of Cognitive Neuroscience, 21: 1146–1161. doi:10.1162/jocn.2009.21097. [PubMed: 18752395]

Rusjan PM, Barr MS, Farzan F, Arenovich T, Maller JJ, Fitzgerald PB, & Daskalakis ZJ (2010). Optimal transcranial magnetic stimulation coil placement for targeting the dorsolateral prefrontal cortex using novel magnetic resonance image-guided neuronavigation. Hum Brain Mapp, 31, 1643–52. doi:10.1002/hbm.20964. [PubMed: 20162598]

Sack AT, Cohen Kadosh R, Schuhmann T, Moerel M, Walsh V, Goebel R (2009) Optimizing functional accuracy of TMS in cognitive studies: a comparison of methods. J. Cogn. Neurosci. 21, 207–221. doi:10.1162/jocn.2009.21126. [PubMed: 18823235]

Shitara H, Shinozaki T, Takagishi K, Honda M, & Hanakawa T (2011). Time course and spatial distribution of fMRI signal changes during single- pulse transcranial magnetic stimulation to the primary motor cortex. Neu- roimage, 56, 1469–79. doi:10.1016/j.neuroimage.2011.03.011.

Siebner HR, Hartwigsen G, Kassuba T, and Rothwell JC. (2009) How does transcranial magnetic stimulation modify neuronal activity in the brain? Implications for studies of cognition. Cortex, 45:1035–1042. doi:10.1016/j.cortex.2009.02.007. [PubMed: 19371866]

Silvanto J, Lavie N, and Walsh V. (2006) Stimulation of human frontal eye fields modulates sensitivity of extrastriate visual cortex. Journal of Neurophysiology, 96: 941–945. doi:10.1152/jn.00015.2006. [PubMed: 16624999]

Speer AM, Willis MW, Herscovitch P, Daube-Witherspoon M, Shelton JR, Benson BE, Post RM, & Wassermann EM (2003). Intensity-dependent regional cerebral blood flow during 1-Hz repetitive transcranial magnetic stimulation (rTMS) in healthy volunteers studied with H215O positron emission tomography: I. Effects of primary motor cortex rTMS. Biol Psychiatry, 54, 818–25. doi:10.1016/S0006-3223(03)00002-7. [PubMed: 14550681]

Strafella AP. Ko JH. Grant J Fraraccio M Monchi O (2005) Corticostriatal functional interactions in Parkinson's disease: a rTMS/[11C]raclopride PET study. Eur J Neurosci, 22(11): 2946–2952. doi:10.1111/j.1460-9568.2005.04476.x. [PubMed: 16324129]

Strafella AP. Paus T Fraraccio M Dagher A (2003) y repetitive transcranial magnetic stimulation of the human motor cortex. Brain, 126(12): 2609–2615. doi:10.1093/brain/awg268. [PubMed: 12937078]

Suarez LE, Markello RD, Betzel RF, Misic B (2020) Linking Structure and Function in Macroscale Brain Networks. Trends Cogn Sci 24, 302–315. [PubMed: 32160567]

Tik M, Hoffmann A, Sladky R, Tomova L, Hummer A, Navarro de Lara L, Bukowski H, Pripfl J, Biswal B, Lamm C, & Windischberger C (2017). Towards understanding rTMS mechanism of action: stimulation of the DLPFC causes network-specific increase in functional connectivity. Neu-roimage, 162, 289–96. doi:10.1016/j.neuroimage.2017.09.022.

Vink JJT, Mandija S, Petrov PI, van den Berg CAT, Sommer IEC, & Neggers SFW (2018). A novel concurrent TMS–fMRI method to reveal propagation patterns of prefrontal magnetic brain stimulation. Hum Brain Mapp, 39, 4580–92. doi:10.1002/hbm.24307. [PubMed: 30156743]

Wang JX, Rogers LM, Gross EZ, Ryals AJ, Dokueu ME, Brandstatt KI, Hermiller MS, and Voss JI (2014) Targeted enhancement of cortical-hippocampal brain networks and associative memory. Science, 345: 1054–1057. doi:10.1126/science.1252900. [PubMed: 25170153]

Wang WC, Wing EA, Murphy DLK, Luber BM, Lisanby SH, Cabeza R, Davis SW, 2018. Excitatory TMS modulates memory representations. Cogn Neurosci 9, 151–166. [PubMed: 30124357]

Weigand A, Horn A, Caballero R, Cooke D, Stern AP, Taylor SF, Press D, Pascual-Leone A, & Fox MD (2018). Prospective validation that subgenual connectivity predicts antidepressant efficacy of transcranial mag- netic stimulation sites. Biol Psychiatry, 84, 28–37. doi:10.1016/j.biopsych.2017.10.028. [PubMed: 29274805]

Zanto TP, Rubens MT, et al. (2011) Causal role of the prefrontal cortex in top-down modulation of visual processing and working memory. Nat. Neurosci 14 (5), 656–661. doi:10.1038\%2Fnn.2773 [PubMed: 21441920]

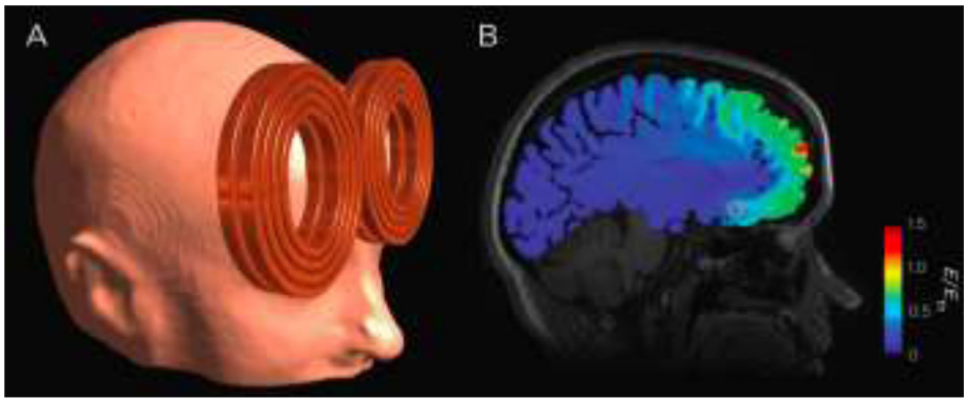

Figure 1.

Representative simulated electric field distribution caused by a TMS pulse. Electric field is superimposed on a sagittal structural MRI slice indicating Brodmann Area 25 (pink circle), a deep brain target of interest in treating depression. Stimulation strong enough to generate action potentials occurs with electric field strength, E, above the estimated neuronal firing threshold, Eth Deng et al. (2011), at the border of yellow and green on the scale. Modeling was performed using the finite element method. The TMS coil (MagVenture MRi-B91) was modeled based on manufacturer data and X-rays of the coil.

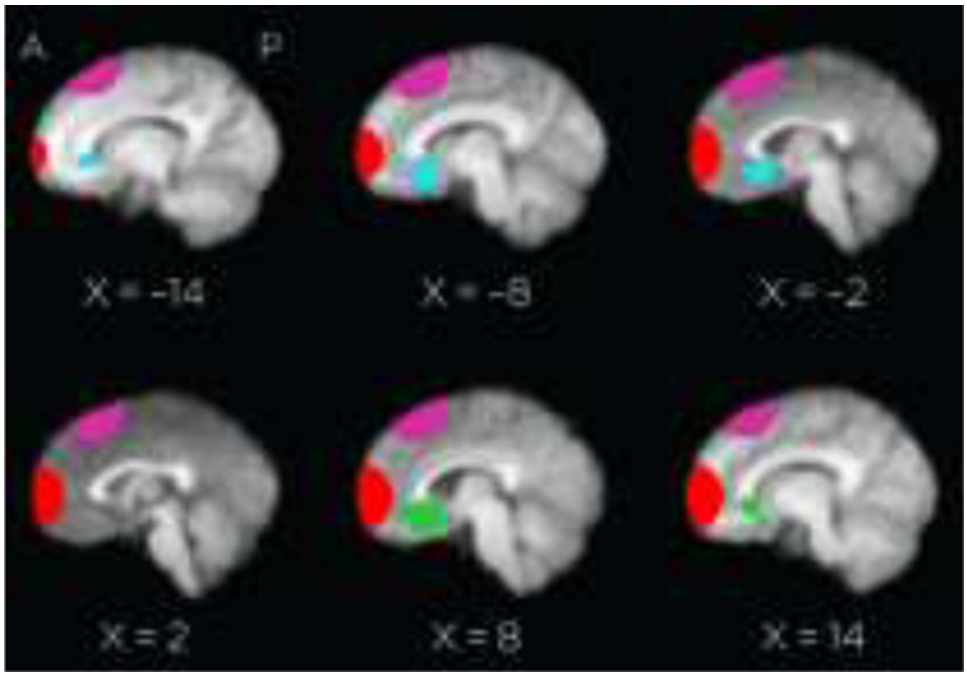

Figure 2.
Four regions of interest used for functional analysis. Red: stimulation site; purple: dorsal control site; green: R-BA25 tractography determined region; blue: L-BA25 tractography determined region.

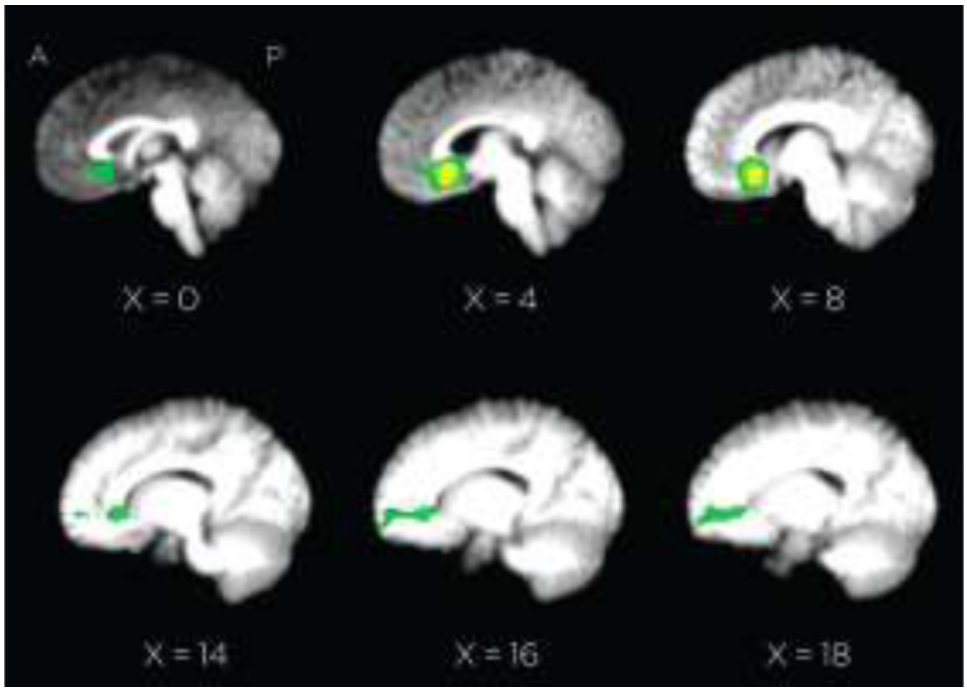

Figure 3.
Group tractography results (FA scores > 3 STD above mean of non-zero voxels). BA25 seed ROI for tractography analysis appears in yellow.

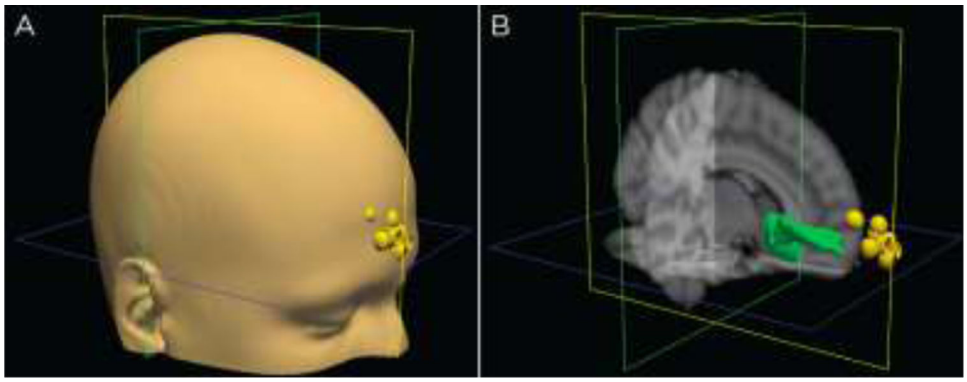

Figure 4.

Coil positions in scanner. Positions are based on fiducial markings. represented for all ten subjects as yellow dots whose coordinates have been transformed to MNI standard space A) on a model head and B) compared to the group averaged DTI tracing (in green).

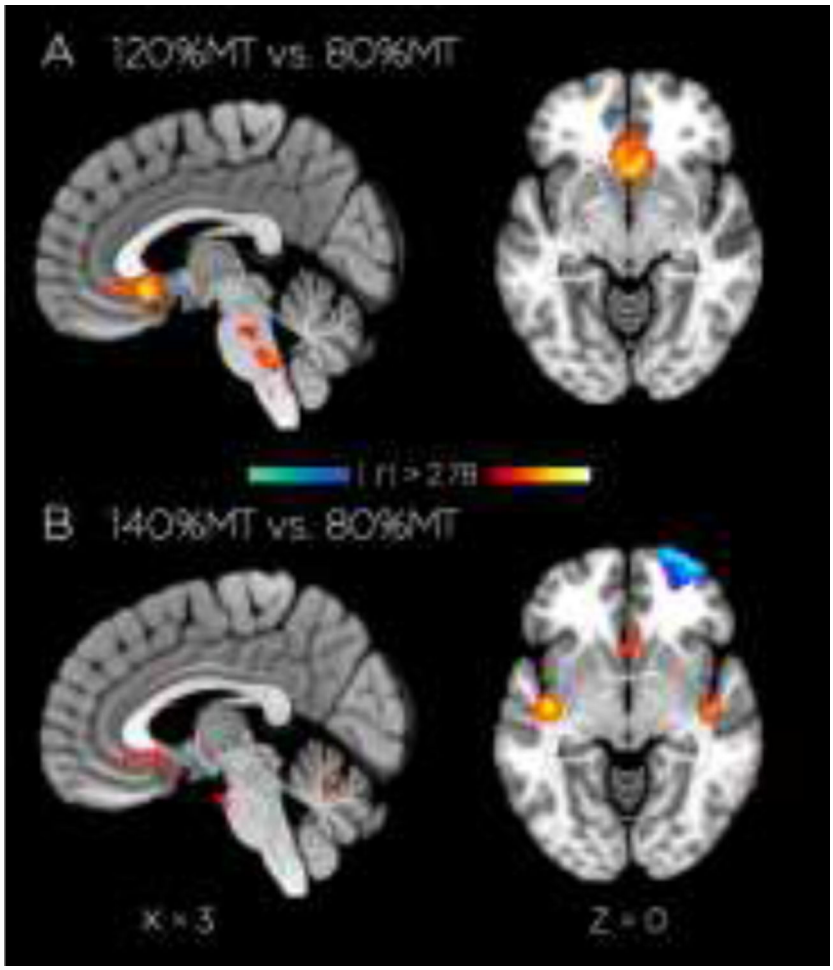

Figure 5.

Stimulation-dependent differences in fMRI-activity. Activation (in red) in right BA25 tractography ROI with a significant ($|t| > 2.78$, cluster significance $p < 0.1$) for transverse ($z = -8$mm to -2mm) and sagittal ($x = 0$ mm to18 mm) slices, contrasting stimulation at A) 120%MT vs 80%MT and B) 140%MT vs 80%MT.

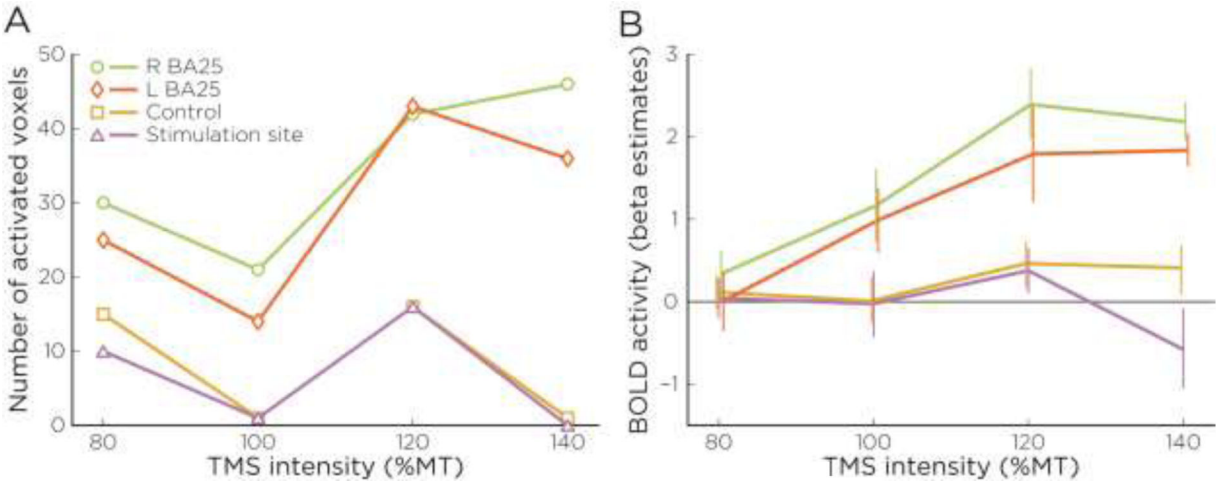

Figure 6:

Group-level Stimulus Effects in Activation. Changes across stimulation intensity (relative to motor threshold) in A) percent of ROI significantly activated for stimulation in all voxels demonstrating a positive effect versus baseline (|t| > 2.78), and B) mean BOLD activity in these same ROIs.

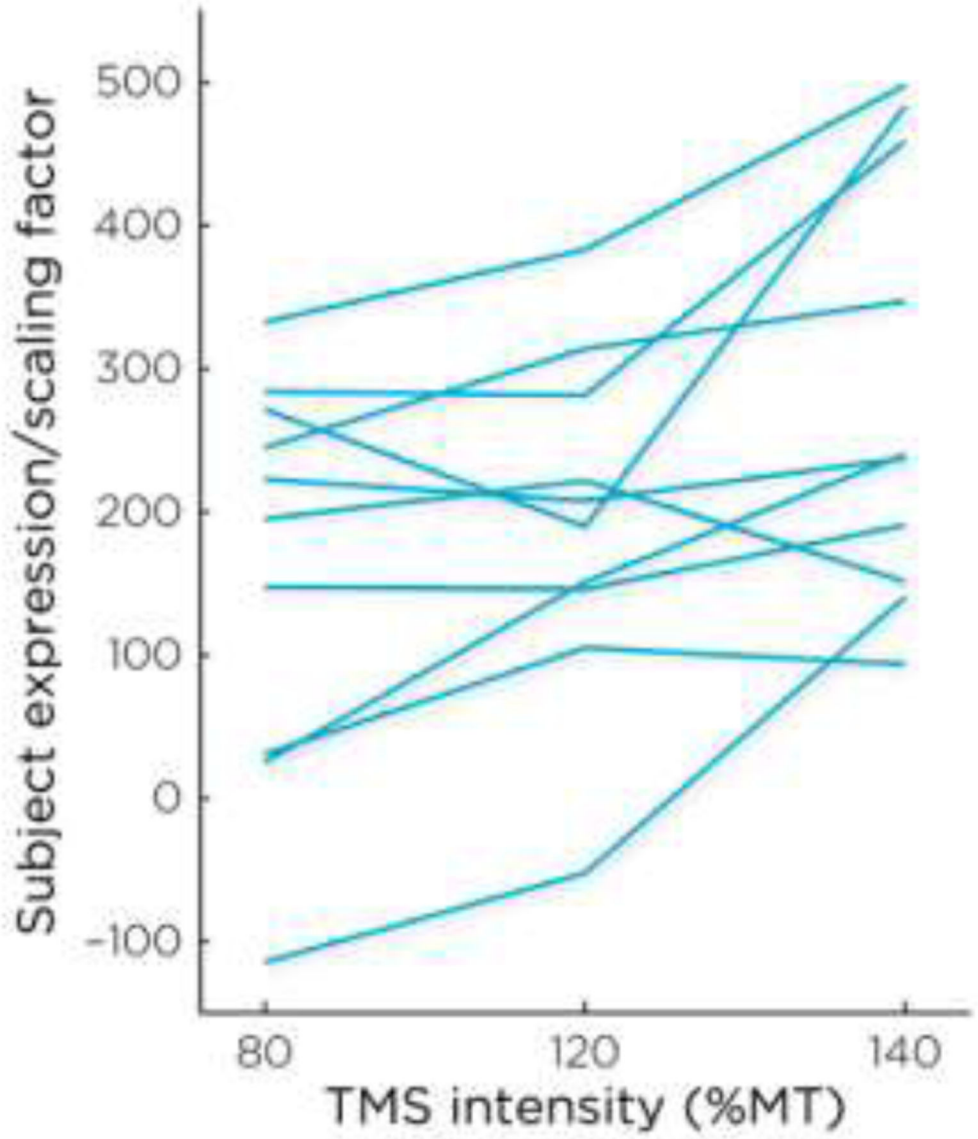

Figure 7.

Subject scores of the best-fit model resulting from the first three principal components of the OrT Analysis. Expression of this model increased across TMS intensity (permutation test: rm- $F=38.66$, $p< 0.03$).

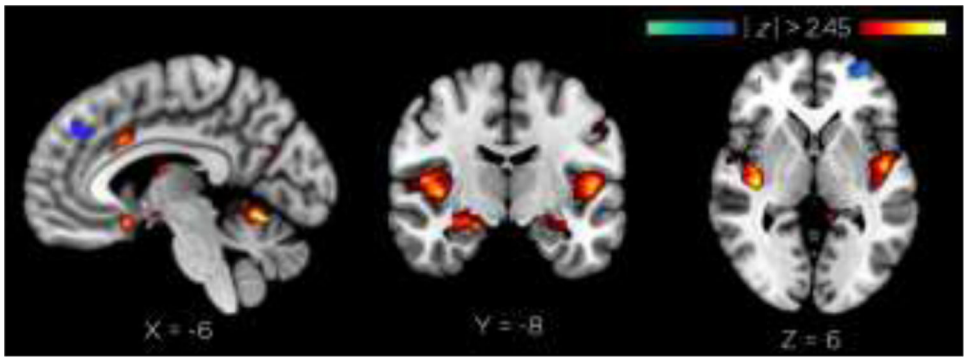

Figure 8.
OrT analysis results. Peak BA25 activation (z = −16mm). Peak BA10 deactivation (MFP z = −2mm).

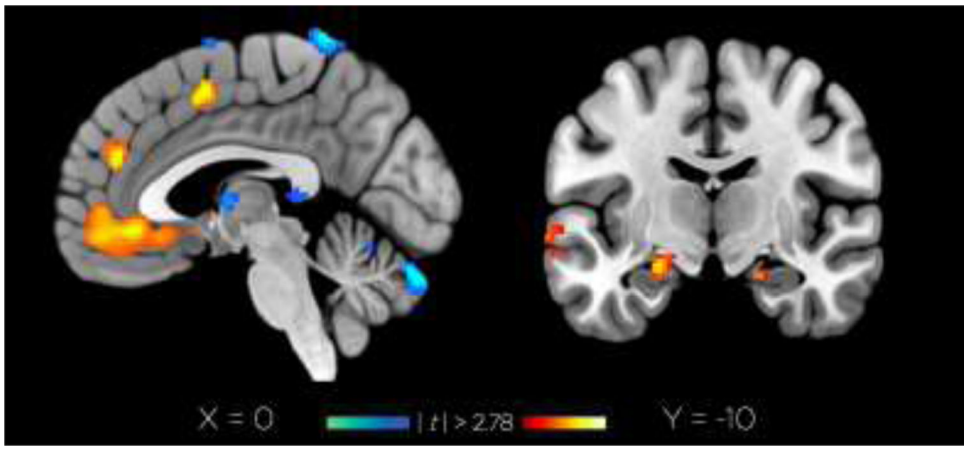

Figure 9.
Group-level effects of seed-based functional connectivity in BA25 (|t| > 2.78).

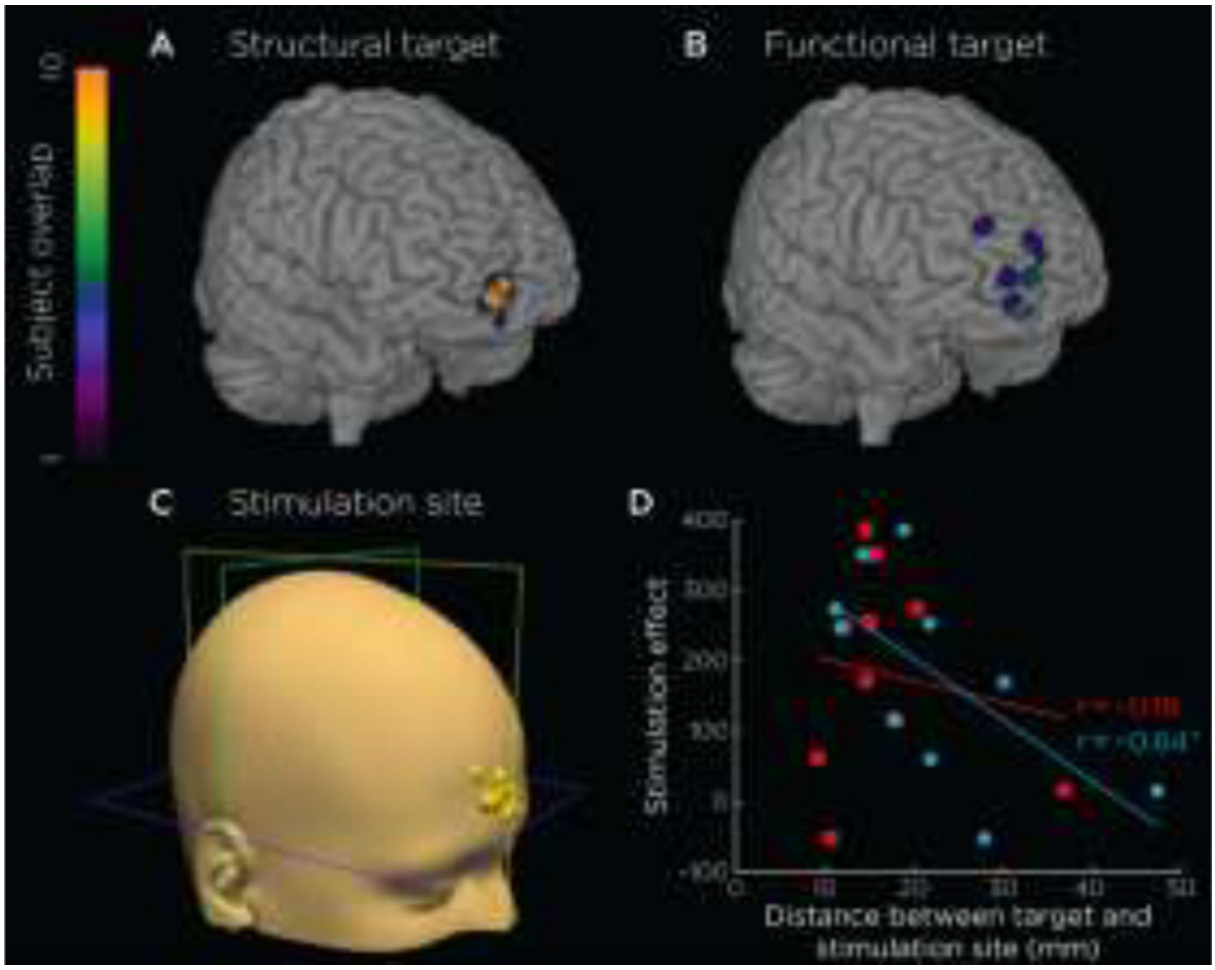

Figure 10.

Efficacy of structural-connectivity-based (A) and functional-connectivity-based (B) targets. Both targets localize to frontal pole, while structural targets provide a more precise target than functionally-defined targets (i.e., lower mean eccentricity). As such, we chose to use structural targets as a basis for localizing the stimulation site for each subject (C). However, despite a significant stimulation effect (> 50) in 80% of subjects, we found a negative relationship with the distance from the stimulation site to the functional target ($r_{10} = -0.64$), shown in D, with blue data points and regression line for functional and red for structural targets. This result suggests that targeting should incorporate both structural and functional targets for DBS targets.

Table 1.

Whole-brain effects of stimulation intensity.

Region	BA	x	y	z	cluster size	*t*
100%RMT vs. 80%RMT						
No significant clusters						
120%RMT vs. 80%RMT						
Subgenual cortex	25	2	20	0	337	3.56
Brainstem		2	−38	−30	102	3.07
140%RMT vs. 80%RMT						
Insula	13	−42	−12	2	276	3.67
Amygdala		14	2	−26	92	3.35
Insula	13	44	−14	4	101	3.10
Frontopolar cortex	10	20	68	8	936	−4.38

Note: Local maxima determined by FSL during cluster analysis ($t > 2.78$, cluster threshold $p < 0.1$) evaluated with the Talairach Daemon Client (http://www.talairach.org/client.html) to determine their nearest Broadman Area within the range indicated in the “Range (mm)” column.

Table 2:

Significantly activated and deactivated (z-scores positive and negative, respectively) regions associated with the best-fit model from the guided PCA analysis.

Region	BA	x	y	z	z-max
Whole brain					
Insula	13	−44	−20	16	5.61
Middle temporal gyrus	21	64	−54	2	3.28
Cingulate gyrus	24	4	10	28	3.02
Cingulate gyrus	24	0	−10	42	2.79
Inferior parietal lobule	40	52	−50	42	2.68
Middle temporal gyrus	21	−60	−56	8	2.79
Cuneus	18	4	−72	22	2.24
Insula	13	52	−32	20	2.11
Middle frontal gyrus	10	32	58	2	−7.13
Postcentral gyrus	40	−46	−32	52	−3.36
Middle temporal gyrus	21	−54	−28	−8	−2.98
Claustrum	*	−28	16	−2	−2.32
Cuneus	18	−4	−88	18	−2.23
Inferior frontal gyrus	47	36	20	−6	−2.06
Inferior frontal gyrus	9	−48	8	28	−2.03
Middle occipital gyrus	19	34	−84	12	−2.02
In DTI ROI					
Medial frontal gyrus	25	10	16	−16	2.41
Medial frontal gyrus	25	10	18	−18	1.66
In BA25 explicit Talairach mask					
Anterior cingulate	25	4	4	−4	2.55
Medial frontal gyrus	25	10	10	−18	2.46
Anterior cingulate	25	2	6	−4	2.15
Medial frontal gyrus	25	12	14	−18	2.06
Anterior cingulate	25	2	2	−4	1.99
Subcallosal gyrus	25	6	12	−14	1.98
Anterior cingulate	25	−2	12	−4	1.92
Anterior cingulate	25	−2	2	−4	1.82

Note: z-scores are estimates based on the bootstrapping procedure described in the Methods. Local maxima determined by FSL during cluster analysis ($t > 2.45$, cluster threshold $p < 0.1$) evaluated with the Talairach Daemon Client (http://www.talairach.org/client.html) to determine their nearest Broadman Area within the range indicated in the “Range (mm)” column.

Table 3.

Regions demonstrating resting functional connectivity with a BA25 seed.

Region	BA	x	y	z	cluster size	*t*
Cerebellum		5	−82	−20	1012	−4.33
Hippocampus		12	−6	−16	85	4.65
Middle temporal gyrus	22	−68	−24	−10	264	4.28
Anterior temporal lobe	38	−60	4	−24	417	4.07
Anterior Cingulate Cortex	24	−2	44	22	231	3.67
Middle Cingulate Cortex	32	−2	6	54	136	3.60
ACC / BA10	10	−6	34	−6	2502	3.44
Hippocampus		−22	−14	−14	143	3.38

Note: Local maxima determined by FSL during cluster analysis ($t > 2.78$, cluster threshold $p < 0.1$) evaluated with the Talairach Daemon Client (http://www.talairach.org/client.html) to determine their nearest Broadman Area within the range indicated in the “Range (mm)” column.